HHS Public Access

Author manuscript

Cell Rep. Author manuscript; available in PMC 2024 February 06.

Published in final edited form as:

Cell Rep. 2023 December 26; 42(12): 113538. doi:10.1016/j.celrep.2023.113538.

MeCP2 represses the activity of topoisomerase IIβ in long neuronal genes

Sabin A. Nettles[1,2], **Yoshiho Ikeuchi**[1,3], **Katheryn B. Lefton**[1], **Ladan Abbasi**[1], **Alyssa Erickson**[1], **Chibueze Agwu**[1], **Thomas Papouin**[1], **Azad Bonni**[1], **Harrison W. Gabel**[1,4,*]

[1]Department of Neuroscience, Washington University School of Medicine, St. Louis, MO 63110, USA

[2]Present address: Department of Pathology, Stanford University, Stanford, CA, USA

[3]Present address: Institute of Industrial Science, The University of Tokyo, Tokyo, Japan

[4]Lead contact

SUMMARY

A unique signature of neurons is the high expression of the longest genes in the genome. These genes have essential neuronal functions, and disruption of their expression has been implicated in neurological disorders. DNA topoisomerases resolve DNA topological constraints and facilitate neuronal long gene expression. Conversely, the Rett syndrome protein, methyl-CpG-binding protein 2 (MeCP2), can transcriptionally repress long genes. How these factors regulate long genes is not well understood, and whether they interact is not known. Here, we identify and map a functional interaction between MeCP2 and topoisomerase IIβ (TOP2β) in mouse neurons. We profile neuronal TOP2β activity genome wide, detecting enrichment at regulatory regions and gene bodies of long genes, including MeCP2-regulated genes. We show that loss and overexpression of MeCP2 alter TOP2β activity at MeCP2-regulated genes. These findings uncover a mechanism of TOP2β inhibition by MeCP2 in neurons and implicate TOP2β dysregulation in disorders caused by MeCP2 disruption.

Graphical abstract

*Correspondence: gabelh@wustl.edu.

AUTHOR CONTRIBUTIONS

Conceptualization, S.A.N. and H.W.G.; methodology, S.A.N. and H.W.G.; formal analysis, S.A.N.; investigation: design, execution, and analysis of all experiments, S.A.N.; IP-MS, Y.I.; RADAR analysis, L.A.; lentivirus production, C.A.; sample preparation, A.E.; *in vivo* eTIP-seq, K.B.L. and T.P.; writing – original draft, S.A.N. and H.W.G.; editing, all authors; supervision, H.W.G., A.B., and T.P.; funding acquisition, H.W.G., A.B., and T.P.

SUPPLEMENTAL INFORMATION

Supplemental information can be found online at https://doi.org/10.1016/j.celrep.2023.113538.

DECLARATION OF INTERESTS

The authors declare no competing interests.

INCLUSION AND DIVERSITY

We support inclusive, diverse, and equitable conduct of research. One or more of the authors of this paper self-identifies as an underrepresented ethnic minority in their field of research or within their geographical location. One or more of the authors of this paper received support from a program designed to increase minority representation in their field of research.

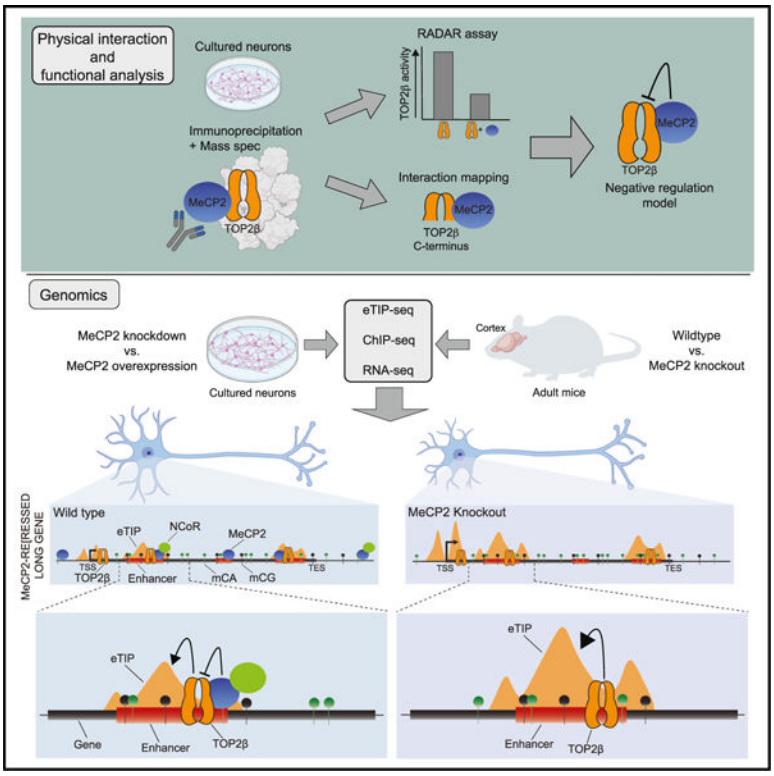

In brief

Nettles et al. establish TOP2β as an MeCP2-interacting protein and demonstrate that MeCP2 negatively regulates TOP2β activity at MeCP2-repressed long genes in neurons. Their results implicate aberrant TOP2β activity in long neuronal genes in the pathology of Rett syndrome.

INTRODUCTION

During development, diverse gene programs establish the complex morphology and connectivity of neurons.[1] The complexity of neuronal transcriptomes is evidenced by the expression of the longest genes in the genome (e.g. >100 kb), which is many folds higher in neurons than in other cell types.[2–4] Many long pre-mRNAs encode essential neuronal proteins, including ion channels, receptors, and adhesion molecules,[2] that have been implicated in neurological disorders.[5] Studies of developing mice and *in vitro*-derived human neurons indicate that expression of long genes is a hallmark of functional maturity,[6,7] and pharmacological interventions that downregulate these genes lead to synaptic and physiological dysfunction.[8] Thus, the expression of long genes is a distinctive feature of neuronal transcriptomes, and disruption of these genes represents a vulnerability to dysfunction in the brain.

Topoisomerase proteins are essential for neural development and critical for long genes.[5,9] These enzymes resolve DNA topological constraints that arise during cell division, gene transcription, and chromatin remodeling.[10–12] Type I topoisomerases (TOP1s) relax DNA by nicking and rejoining one DNA strand, whereas type II topoisomerases (TOP2s) break

and rejoin both DNA strands.[13–16] Mammalian cells express two TOP2 enzymes, TOP2α and TOP2β. Although these enzymes have similar structures and activities, their expression and biological roles differ.[17,18] TOP2α is expressed in proliferating cells but not neurons, whereas TOP2β is expressed in dividing and post-mitotic neurons.[19–25] Deletion of *Top2b* leads to defective brain development,[26,27] and pharmacological inhibition or knockdown (KD) of TOP2β in cultured neurons reduces long-gene expression.[5] While the mechanisms by which TOP2β promotes gene expression are not clear, TOP2β may decatenate DNA, opening chromatin and activating regulatory regions,[28,29] or unwind DNA to aid RNA polymerase processivity.[4,5,8] These studies indicate that TOP2β is critical for robust expression of long genes and essential for brain function.

Balanced gene expression is essential, and studies have implicated methyl-CpG-binding protein 2 (MeCP2) as a modulator of neuronal transcription that preferentially downregulates long genes.[2,3,30–33] MeCP2 loss or overexpression (OE) causes Rett syndrome[34] or MeCP2-duplication syndrome,[35] respectively, demonstrating its importance in the brain. Although multiple functions of MeCP2 have been described, molecular and genomic analyses suggest MeCP2 binds to methylated DNA within and around genes to promote repressive chromatin structure, downregulating transcription. Transcriptional repression by MeCP2 appears to be mediated in part by downregulation of enhancers within genes, leading to reduced transcription initiation.[31,36–39] Notably, because long genes are enriched for DNA methylation and contain many enhancers, these repressive effects most robustly affect long genes, with critical functions in neuronal development and physiology.[2,3,40] These studies suggest that an important function for MeCP2 is to tune down long gene expression and implicate disruption of this mechanism in the pathology of MeCP2-associated disorders.

Mechanistically, biochemical studies have identified protein interactors of MeCP2 that may mediate its functions. Extensive evidence suggests that MeCP2 functions as a repressor by interacting with the NCoR/SMRT co-repressor complex.[36] In addition, PSIP1/LEDGF and TCF-20 likely play roles in MeCP2-mediated gene regulation.[41,42] However, whether additional protein interactors or mechanisms play a key role in MeCP2 functions remains to be investigated.

Here, we uncover an interaction between MeCP2 and TOP2β with functional implications for long genes in neurons. We identify and interrogate a physical association between TOP2β and MeCP2, implicating a key domain of MeCP2 in this interaction. We profile sites of TOP2β activity in neurons genome wide and determine that TOP2β is preferentially active at long genes. We demonstrate that disrupting MeCP2 levels in neurons alters TOP2β activity at long, MeCP2-regulated genes. Thus, the interaction between TOP2β and MeCP2 regulates essential neuronal genes, and disruption may contribute to MeCP2-related neurological disorders.

RESULTS

MeCP2 selectively binds and modulates the activity of TOP2β

To explore mechanisms underlying MeCP2 long-gene regulation, we sought to identify additional MeCP2 protein interactors. We expressed and purified FLAG-tagged MeCP2 protein in mouse cultured cortical neurons and performed mass spectrometry analysis of co-precipitating proteins (Table S1). In addition to previously described MeCP2 interactors (KPNA3 and PSIP1/LEDGF),[36,42–44] multiple additional proteins were reproducibly identified (Figure 1A; Table S1). For example, we detected DHX30, an RNA helicase that results in a developmental disorder similar to Rett syndrome when mutated.[45,46] The splicing factor SFRS14 was also detected and may contribute to MeCP2 splicing-regulatory functions.[42] Notably, TOP2β was reproducibly identified in this analysis. Motivated by previous separate studies showing that inactivation of topoisomerase enzymes[5] and MeCP2 mutation[2] lead to opposing effects on long genes, we focused further investigation on this interaction.

To independently test TOP2β-MeCP2 association in the brain, we immunoprecipitated MeCP2 from forebrain extracts of wild-type 8-week-old mice. To eliminate potential nucleic acid bridging, nuclear extracts were treated with benzonase, a DNA-RNA nuclease, before immunoprecipitation (IP) was carried out. This analysis revealed co-immunoprecipitation (coIP) of TOP2β but not TOP1, the other major topoisomerase robustly expressed in brain (Figure 1B). This validated interaction between MeCP2 and TOP2β suggests that modulation of long-gene expression by MeCP2 may involve alterations in the activity of TOP2β.

MeCP2 and TOP2β are highly conserved in vertebrate species and well characterized, with specific protein domains defined for distinct protein functions.[36,37,39,47–52] We therefore established a coIP assay in heterologous cells to ask which protein sequences are sufficient for the interaction. Co-expression of MYC-tagged full-length (1–1,612 aa) TOP2β with FLAG-tagged full-length (1–484 aa) MeCP2 in HEK293 cells led to a detectable coIP (Figure 2A). Notably, this interaction was specific, as expression of MYC-tagged full-length TOP2β with another nuclear protein, FLAG-tagged DNMT3A, had no detectable coIP signal.

Having validated the assay, we probed which TOP2β sequences are sufficient for interaction with MeCP2. TOP2β contains three functional regions: the amino-terminal ATP-binding domain allows dimerization between TOP2 monomers, the central catalytic domain is responsible for strand breakage and re-ligation, and the carboxyl-terminal region is implicated in localization and regulation of enzyme activity.[16–18,52–56] Co-expression of MYC-tagged N-terminal (1–449 aa), central catalytic (450–1,198 aa), and C-terminal (1,199–1,612 aa) fragments with FLAG-tagged full-length MeCP2 (1–484 aa) in HEK293 cells resulted in coIP of MeCP2 specifically with the C-terminal region (CTR) of TOP2β (Figure 2B). The interaction of MeCP2 with the CTR of TOP2β is notable because the CTRs differ between TOP2α and TOP2β and are proposed to give rise to the unique functions of these related topoisomerases.[57–59]

We next interrogated MeCP2 regions sufficient for interaction with TOP2β. MeCP2 contains two major domains: the methyl-DNA-binding domain (MBD) and the NCoR-interaction domain (NID).[36,37,39,47,60,61] A minimal protein containing these two domains rescues Rett syndrome-like effects caused by MeCP2 mutation in mice.[62] Co-expression of FLAG-tagged MeCP2 fragments containing the MBD (1–167 aa), spanning the MBD and NID (143–484 aa), or containing the C terminus (384–484 aa) with MYC-tagged full-length TOP2β (1–1,612 aa) results in efficient coIP of the 1–167 and 147–484 aa MeCP2 fragments with TOP2β, while the MeCP2 C terminus did not interact (Figure 2C). These results suggest that TOP2β interacts with the MBD of MeCP2. Notably, this is a key domain for Rett phenotype rescue, suggesting that loss of TOP2β interaction could contribute to Rett syndrome.

Given the MeCP2 and TOP2β association, we sought to assess if MeCP2 regulates TOP2β function. To assay TOP2β activity in cells, we performed the rapid approach to DNA adduct recovery (RADAR) assay,[63] in which HEK293 cells are transfected with TOP2β and treated with etoposide to quantify DNA cutting by the enzyme. Etoposide is a TOP2 inhibitor that traps the enzyme in a covalently linked complex with cleaved DNA during the cutting and re-ligation cycle.[64,65] After etoposide treatment, cells are lysed, and the DNA is stringently purified to remove all non-covalently linked proteins and slot blotted. TOP2β immunoblotting then reports the level of DNA cutting that was occurring genome wide in the treated cells. RADAR analysis showed that TOP2β activity was globally reduced by the overexpression of MeCP2 (Figures 2D–2F), suggesting that MeCP2 interacts with TOP2β to negatively regulate its topoisomerase activity.

TOP2β activity is enriched within long genes in neurons

In light of our finding that MeCP2 interacts with and reduces the activity of TOP2β, we next investigated genomic sites of action for TOP2β and assessed the impact of MeCP2 on this function. Previous analyses have shown that TOP2β KD in neurons causes reduced long-gene expression, but where TOP2β acts to facilitate long gene transcription is not well understood. We therefore performed etoposide-mediated topoisomerase IP sequencing (eTIP-seq)[66] in mouse primary cortical neurons. In this genomic profiling assay, as in RADAR, etoposide is used to trap topoisomerase on DNA at sites where it is active. The DNA is stringently purified to remove non-covalently linked protein and sonicated, followed by TOP2β IP and sequencing of isolated DNA to profile enzyme activity across the genome (Figure 3A). In contrast to conventional chromatin IP (ChIP), which uses formaldehyde to cross-link protein to DNA and profile genomic binding, employing eTIP allowed us to directly assess TOP2β activity in neurons and study how MeCP2 affects TOP2β activity.

We first performed eTIP-seq in cultured cortical neurons at day *in vitro* 12 (DIV12), where we could administer etoposide directly to the cells (Figure 3A). Isolation of DNA by eTIP yielded robust levels of immunoprecipitated DNA compared with vehicle (DMSO)-treated controls, which recovered insufficient DNA for sequencing, indicating high assay specificity (Figure S1A; Table S5). eTIP-seq profiles revealed enriched TOP2β activity at annotated promoters and gene bodies compared with input controls. Notably, eTIP-seq signal appeared to be higher at longer genes (>100 kb) relative to shorter genes (Figure 3B). To quantify TOP2β activity, we performed aggregate analysis and quantification of

signal at promoters and gene bodies. Aggregate plots showed that TOP2β is consistently associated with promoter regions, with the signal peak spanning +1 to +3 kb relative to the transcription start site (TSS), hereafter referred to as “promoter-associated” signal (Figure 3C). Aggregate plots of genes by length revealed enrichment of TOP2β at promoter-associated regions and gene bodies of long genes compared with shorter genes (Figures 3C and S1B). Quantification of TOP2β signal verified aggregate profiles, showing a robust correlation between TOP2β enrichment and gene length (Figures 3D, S1B, and S1C; Tables S2 and S3).

Since long genes are robustly expressed in neurons, we therefore assessed if TOP2β signal at genes is correlated with gene expression, and if so, whether this association explains enrichment of TOP2β at long genes. We performed RNA-seq analysis on neuronal cultures at the same time point as eTIP-seq and assessed TOP2β enrichment relative to gene expression (Figure S1F). This analysis showed a modest association between expression level and TOP2β enrichment at genes. Notably, however, while long genes are robustly expressed in our cultured neurons, they are not more highly expressed than shorter genes (Figure S1G; Table S3). In addition, quantification of eTIP signal across gene length for a subset of genes selected to have similar, moderate expression levels revealed gene-length-associated TOP2β enrichment, even in this expression-controlled analysis (Figure S1H). These findings indicate that TOP2β activity is associated with mRNA levels, but that TOP2β recruitment to long genes is not explained by expression.

We noted sites of eTIP-seq enrichment outside of promoter regions reminiscent of peaks associated with enhancers (Figure 3B) and therefore investigated TOP2β signal at these distal regulatory regions. To define putative enhancers, we performed ChIP-seq on histone H3 lysine 27 acetylation (H3K27ac), a histone modification associated with active promoters and enhancers. We performed peak calling on these H3K27ac data and assessed overlap of eTIP signal with acetyl peaks outside of TSSs (Table S4). eTIP profiles showed enriched TOP2β signal for enhancers found both inside and outside of genes (Figures 3B and 3E; Table S4). Notably, TOP2β enrichment was higher at enhancers located within genes (intragenic) relative to enhancers outside of genes (extragenic). This increased enrichment at intragenic enhancers may partially explain increased signal inside long genes containing many enhancers.

To independently assess TOP2β activity profiles in an unbiased manner, we performed peak calling on the TOP2β eTIP-seq signal. We assessed where these peaks land in the genome, comparing them with re-sampled controls. This analysis revealed that TOP2β peaks are significantly more prevalent within intragenic regions than within extragenic regions compared with controls (Figure S1D; Table S4). Analysis of TOP2β peak overlap with promoters and putative enhancers, as defined by H3K27ac above, indicated that TOP2β peaks are significantly enriched within promoters and enhancers and are further enriched within intragenic enhancers compared with extragenic enhancers (Figures 3F and 3G; Table S4). Together, the results of this peak distribution analysis are consistent with TOP2β enrichment within genes and intragenic enhancers described above (Figure 3E; Table S4). Our analysis of TOP2β peaks revealed additional TOP2β peaks in unannotated regions (Figure S1E; Table S4). Many of these sites may be enhancers that were just below the level

of detection of the H3K27ac peak-calling analysis. However, many may not be enhancers. Notably, nearly two-thirds of the unannotated TOP2β peaks are intragenic, suggesting TOP2β is engaged and active at many sites within these genes.

Standard eTIP analysis is performed with a high concentration etoposide (500 μM) in a brief treatment protocol (15 min) to rapidly capture TOP2β molecules engaging the genome.[66] To further characterize TOP2β activity, we repeated our analysis using a lower drug concentration (50 μM for 30 min) and detected similar eTIP-seq profiles across promoters and enhancers genome wide (Figures S1I–S1K). However, we did not detect enrichment within non-enhancer regions of gene bodies for long genes (Figures S1I and S1J). This may result from less efficient capture of TOP2β at sites of lower-level activity using the reduced drug concentration.

To further probe the validity of our findings, we performed eTIP-seq using an independent TOP2β antibody targeting a different protein region. Consistent with initial observations, the second antibody yielded TOP2β enrichment at promoter-associated regions and gene bodies of long genes, as well as at enhancers (Figures S2A–S2D; Table S4). Peaks detected genome wide showed similar co-localization within promoters and enhancers, particularly intragenic enhancers, with TOP2β peaks also observed in unannotated regions (Figures S2E–S2H; Table S4). These analyses confirm TOP2β enrichment at promoters and enhancers within long genes, suggesting that the activity of TOP2β at these regulatory regions may play an important role in the transcription of these genes.

Activity of TOP2β on the genome requires both the close association of the enzyme with the genome and the initiation of DNA cutting. We therefore assessed the binding of the enzyme via ChIP-seq analysis. TOP2β ChIP-seq revealed enriched binding at promoters and enhancers in neurons that was consistent with the enriched enzyme activity measured at these sites (Figures 3B and 3H–3J). Enriched binding was also observed at the promoters of long genes (Figures 3H, 3I, and S3A). This signal was less prominent than signal detected in eTIP-seq (Figures 3C and 3D), however, suggesting the enzyme is also differentially active at these genes rather than simply binding more. While intragenic enhancers were enriched for TOP2β ChIP signal, gene-body ChIP-seq signal in general was not significantly higher in longer genes (Figure S3A). This suggests that differential activity alone, as captured by eTIP-seq, is occurring within long gene bodies, rather than enriched binding. Alternatively, the gene body signal outside of intragenic enhancers may be unique to high-concentration eTIP-seq.

MeCP2 regulates TOP2β activity at long genes repressed by MeCP2

Given the MeCP2-TOP2β interaction, together with the opposing effects of MeCP2 and TOP2β on long gene expression, we next investigated if MeCP2-regulated long genes are targets of TOP2β and if MeCP2 modulates the activity of TOP2β at these genes. Analysis of eTIP-seq signal at “MeCP2-repressed” genes, a set of long genes consistently upregulated when MeCP2 levels are low and downregulated when MeCP2 levels are high across multiple *in vivo* MeCP2 mutant studies,[2] revealed TOP2β enrichment at the promoter-associated regions and gene bodies of these genes. This signal was enriched relative to unchanged genes and “MeCP2-activated” genes, a gene set with opposite dysregulation in MeCP2

mutants[2] (Figures 4A and 4B; Table S3). TOP2β enrichment at MeCP2-repressed genes was not explained by gene expression levels (Figure S4A), but rather was likely driven by recruitment of TOP2β due to the long length of these genes. In support of additional physical recruitment to these long genes, ChIP-seq analysis also detected enrichment of TOP2β at MeCP2-repressed genes (Figure S3B), and similar enrichments occurred in eTIP-seq performed with low-concentration etoposide (Figure S4B). In contrast, MeCP2-activated genes displayed modest TOP2β enrichment relative to unchanged genes (Figures 4A, 4B, S4A, and S4B), which may stem from their higher expression level (Figure S4A). Altogether, these findings indicate that MeCP2-repressed genes, like other long genes, are major targets of TOP2β.

Given that MeCP2 preferentially downregulates a subset of neuronal long genes (e.g., MeCP2-repressed genes), we hypothesized that TOP2β recruited to long genes may be negatively regulated by MeCP2 to restrict expression of these genes. To address this question, we performed KD or OE of MeCP2 in primary cortical cultures and carried out gene expression and eTIP-seq analyses (Figure 4C; Table S3). Because MeCP2 protein increases dramatically during post-natal development,[67,68] these cultures contain low levels of MeCP2 compared with the adult brain. Thus, we overexpressed MeCP2 in these cells to model the role of MeCP2 in the mature brain. We paired this with MeCP2 KD to remove low levels of MeCP2 and better recapitulate Rett syndrome-like conditions, in which no MeCP2 activity is present in neurons. Assessment of MeCP2 RNA levels in MeCP2-KD and MeCP2-OE conditions revealed robust reduction of endogenous MeCP2 and significantly higher MeCP2 expression, respectively (Figure 4D; Table S5). To assess if our culture system mirrors the MeCP2-mediated gene regulation observed in the brain, we performed total RNA-seq on the MeCP2-KD and MeCP2-OE cultured neurons. Differential gene expression analysis showed that MeCP2-repressed genes previously identified in the *in vivo* studies of multiple brain tissues[2] were significantly upregulated in MeCP2-KD neurons, and MeCP2-activated genes were significantly downregulated (Figure S4C; Table S3). Thus, our manipulation of MeCP2 in the cultured neurons elicits changes in gene expression that are consistent with the changes observed in the brain and therefore provides a suitable context to assess how MeCP2 affects TOP2β activity in neurons.

Having established our culture system, we performed eTIP-seq in the MeCP2-KD and MeCP2-OE conditions to test if loss of MeCP2 induces an increase in TOP2β activity at long, MeCP2-repressed genes. Visualization of the eTIP signal at these genes suggested higher TOP2β activity in MeCP2-KD neurons compared with MeCP2-OE neurons (Figure 4E; Table S3). To quantify changes in eTIP signal at MeCP2-regulated genes, we performed differential analysis of eTIP reads and examined the population of genes that was previously identified as both MeCP2 repressed in *in vivo* studies and differentially expressed across MeCP2-KD and MeCP2-OE neurons (Figures 4F and S4C–S4E). This analysis revealed increased TOP2β activity at promoter-associated regions and gene bodies of MeCP2-repressed genes in MeCP2-KD compared with MeCP2-OE (Figure 4G; Table S3). Similar trends were observed when analyzing all genes significantly changed across the KD and OE conditions or all genes identified in *in vivo* studies (Figures S4C–S4F). Consistent with higher, adult-brain-relevant levels of MeCP2 causing TOP2β repression, we detected reduced eTIP signal at MeCP2-repressed genes in MeCP2-OE neurons compared with

unmanipulated control neurons. In contrast, inconsistent effects were observed in MeCP2-KD compared with controls, where MeCP2 levels were low in both conditions (Figure S4G). At MeCP2-activated genes, TOP2β activity showed limited changes in signal (Figures 4G and S4F).

One mechanism by which MeCP2 regulates long gene expression is by repressing the activity of intragenic enhancers associated with these genes.[40] We therefore evaluated the eTIP signal at intragenic enhancers of MeCP2-regulated genes[2] in MeCP2-KD and MeCP2-OE neurons. TOP2β activity showed subtle, but significant, increases at these enhancers in MeCP2-KD compared with MeCP2-OE (Figure 4H; Table S4), suggesting that negative regulation of TOP2β by MeCP2 contributes to intragenic enhancer repression.

To further interrogate MeCP2 regulation of TOP2β, we performed ChIP-seq analysis in MeCP2-KD and -OE neurons. This analysis revealed subtle alterations in DNA association that mirrored TOP2β activity changes detected by eTIP (Figures S3C and S3D), with TOP2β ChIP increased at promoters and gene bodies of MeCP2-repressed genes in MeCP2-KD compared with MeCP2-OE. These effects may result from TOP2β making closer contacts with the DNA in the absence of MeCP2 or reflect increased DNA cutting resulting in more efficient cross-linking in the ChIP assay.

While our findings indicate that MeCP2 can regulate TOP2β activity in cultured neurons, the major functions of MeCP2 *in vivo* emerge as the protein and one of its major binding sites, DNA methylation at CA dinucleotides (mCA), accumulate in the mature brain.[69] We therefore evaluated the impact of MeCP2 in this context by implementing eTIP-seq analysis in *ex vivo* adult mouse cortex. Acute cortical slices from 8-week-old wild-type and MeCP2-knockout (KO) mice were treated with etoposide or vehicle control and processed for eTIP-seq as with cultured neurons. This procedure resulted in etoposide-dependent capture of DNA (see STAR Methods), and eTIP-seq revealed profiles of enrichment at promoters and enhancers genome wide (Figures 5A–5C). Promoter-associated eTIP signal was correlated with gene length (Figures 5A, 5B, and 5D), and MeCP2-repressed genes were enriched for eTIP signal within promoters and gene bodies (Figures 5E and 5F). Loss of MeCP2 resulted in a subtle but significant eTIP signal increase at MeCP2-repressed genes (Figures 5A and 5G), as well as enhancers previously identified as MeCP2 regulated[40] (Figure 5H). Notably, these effects correspond to enriched mCA and MeCP2 binding at MeCP2-repressed genes (Figure S5), suggesting that regulation is mediated through MeCP2 recruitment to mCA. In further support of MeCP2 regulation of TOP2β through DNA-methylation binding, we found that changes in eTIP signal at enhancers genome wide correlated with DNA-methylation levels atthese sites (Figure 5I). These effects mirror similar genome-wide impacts on enhancer activity detected in MeCP2 KO.[40] Together these analyses demonstrate that MeCP2 mutation leads to altered TOP2β activity in mature brain and implicate these alterations in Rett syndrome.

DISCUSSION

Here, we have established a MeCP2-TOP2β interaction in neurons and demonstrated its importance for modulating TOP2β activity at MeCP2-regulated long genes. One model

consistent with our findings is that, when neurons are born, TOP2β is recruited to long genes, including MeCP2-repressed genes, through MeCP2-independent mechanisms. This binding facilitates essential long gene expression in neurons. As neurons mature post-natally, MeCP2 becomes highly expressed and interacts with TOP2β at long, highly methylated genes to act as a molecular brake on TOP2β activity, tempering gene expression. Loss of MeCP2, as in Rett syndrome, disrupts this molecular brake, allowing TOP2β activity to become unrestricted within long, MeCP2-regulated genes (Figure 6). This regulation may be critical to the role of MeCP2 in tuning neuronal gene expression.

TOP1 and TOP2 enzymes both promote the expression of long genes by resolving topological constraints. Removal of these enzymes in neurons results in subtle reductions in long gene expression, with TOP1 loss affecting these genes more than TOP2β loss.[5] Our analysis shows that MeCP2 binds uniquely to TOP2β, but not the TOP1. In addition, we show that MeCP2 interacts with the CTR of TOP2β. Structural studies indicate that the CTR is the most divergent region between TOP2β and TOP2α, which is expressed in dividing cells but not neurons. While removal of the CTR of TOP2β does not affect catalytic activity,[16,57] CTR truncation does cause increased binding of TOP2β to DNA, suggesting this region has a negative regulatory function.[58,59] These observations provide evidence that CTR regulatory function may be modulated by MeCP2 binding. Notably, the expression and specialization of TOP2β, TOP2α, and MeCP2 have emerged in the vertebrate lineage[16,71] and therefore may contribute to regulation of complex vertebrate neuronal transcriptomes.

Our mapping of MeCP2 fragments sufficient for TOP2β binding implicates this interaction in Rett syndrome. We show the TOP2β interaction occurs with MeCP2 fragments that contain the C-terminal portion of the MBD. Structural studies indicate that this portion of the MBD is outside of the region directly contacting DNA,[37] suggesting that MeCP2 can regulate TOP2β while bound to DNA. Previous studies identified two critically important functional domains of MeCP2 that contain Rett-causing missense mutations, the MBD and the NID.[36,37,62] The MBD is required for interaction with methylated DNA,[2,33,60,61] while the NID is required for interaction with the NCoR-co-repressor complex.[36] Our findings suggest the need to evaluate the effects of Rett syndrome missense mutations in the MBD, as some may disrupt TOP2β interaction rather than solely disrupting methyl-DNA binding.

While it is not known how TOP2β facilitates long gene expression, our study uncovers TOP2β activity at promoters and enhancers of long genes that may provide insight into this mechanism. Neuronal eTIP-seq specifically recovers TOP2β enzymes during cutting of DNA, thereby associating functional relevance to each enriched site. Previous ChIP-seq studies in neurons observed TOP2β enrichment at actively transcribed genes, promoters, and regions of open chromatin and adjacent to genes encoding ion channels and receptors.[19,66,72] Here, we report a genome-wide gene-length-associated enrichment of TOP2β activity in neurons. Future studies can assess how TOP2β activity is targeted specifically to longer genes and what role it plays in facilitating expression of these genes.

MeCP2 has been characterized as a repressor, given its binding to methylated DNA and recruitment of the NCoR-co-repressor complex. Disruption of MeCP2 causes dysregulation of intragenic enhancers and upregulation of long, highly methylated genes, which may

contribute to Rett syndrome pathology.[31,40] By profiling TOP2β genome wide in neurons that have low initial levels of MeCP2, we find that TOP2β enrichment occurs at promoter-associated regions and gene bodies of long, MeCP2-repressed genes prior to the accumulation of MeCP2. Manipulating MeCP2 expression in cultured neurons or in the adult brain alters the activity of TOP2β at MeCP2-regulated genes in a manner that is consistent with MeCP2 inhibiting TOP2β at these sites. Thus, TOP2β targeting of long genes does not appear to require MeCP2; rather, its activity at these sites is modulated by interaction with MeCP2 in mature neurons.

Because MeCP2 has no catalytic domain, it is hypothesized to function as a bridge between chromatin and the NCoR-co-repressor complex.[73] One possible model for this function in regulating TOP2β is that MeCP2 recruitment of the NCoR complex inhibits TOP2β activity. The NCoR complex contains a histone deacetylase (HDAC3), which could deacetylate TOP2β to regulate its activity, in addition to affecting histone substrates. In this model, Rett syndrome mutations might affect TOP2β modulation by directly disrupting the interaction between MeCP2 and TOP2β or, for example, in the case of the well-characterized R306C mutation,[73] by blocking NCoR recruitment and leading to loss of TOP2β negative regulation. Future studies can test this model by investigating whether TOP2β acetylation is altered in MeCP2 mutants.

While numerous studies have built a molecular model of gene repression by MeCP2 and NCoR,[36,74] direct mechanisms affecting MeCP2-activated genes upon loss of MeCP2 are not as well defined. In some analyses here, we observe a subtle reduction of TOP2β activity at MeCP2-activated genes upon loss of MeCP2. These alterations may represent the loss of a TOP2β-activating function of MeCP2. Alternatively, because differential count analysis pipelines re-balance effects genome-wide based on assumption of similar count distributions across samples, the apparent reduced signal may represent a relative lack of TOP2β de-repression at MeCP2-activated genes when MeCP2 is lost.

Outside of gene expression, our findings, combined with other studies, suggest that MeCP2-TOP2β interaction should be investigated as a modulator of DNA damage in neurons. TOP2β cuts DNA to modify topology, and if it is disrupted during this process, aborted cutting and ligation cycles can results in double-stranded breaks (DSBs). Because long genes experience topological constraints that do not affect shorter genes, they may require higher levels of TOP2β activity to resolve these constraints and be prone to DSBs. MeCP2 may be required to maintain TOP2β activity at optimal levels in these genes, and when MeCP2 is absent, TOP2β may be overactive, giving rise to errors and increased DSBs. Notably, previous studies have reported recurrent DSBs in long genes in neural progenitors[75] and detected increased DSBs in neural progenitor cells from *Mecp2*-KO mice.[76] Furthermore, a recent genetic suppressor screen for mutations that ameliorate Rett-like phenotypes in MeCP2-KO mice detected mutations in DNA damage-response-pathway genes. This includes RBBP8, a protein that regulates the repair of TOP2-induced DSBs,[77] suggesting that altering DSB pathways affected by TOP2β dysfunction modifies Rett-like phenotypes. Our findings of TOP2β regulation by MeCP2 may provide an underlying mechanism to explain these genetic findings and motivate studies to explore the presence of TOP2β-induced DSBs in MeCP2 mutants.

Altogether, we have identified a TOP2β-MeCP2 molecular interaction in neurons associated with the regulation of neuronally enriched long genes. Future studies can investigate the mechanism and functional importance of this interaction, as well as the degree to which it is disrupted by Rett syndrome mutations in MeCP2. Such studies may reveal potential therapeutic strategies for MeCP2-related disorders, such as small molecules that reduce TOP2β activity.

Limitations of the study

While our mass spectrometry study discovers an interaction between MeCP2 and TOP2β that we confirm and evaluate functionally, our detection of interactors appears to be incomplete, as known interactors such as NCoR components[36,74] were not detected. The sensitivity of coIP mass spectrometry studies is often dependent on protein expression levels, tagging methods and location, and sample preparation procedures. Thus, the results from our analysis should not be interpreted as a full characterization of the MeCP2 interactome.

Here, we utilize RADAR, eTIP-seq, and ChIP-seq analysis to show that MeCP2 expression leads to changes in TOP2β activity and genome binding. However, we do not define molecular mechanisms of MeCP2-mediated TOP2β repression. Future studies can further dissect the domains required for this physical and functional interaction and assess the impacts of Rett syndrome-associated mutations on TOP2β.

While our eTIP-seq approach reports TOP2β activity profiles that are validated by negative controls and corroborated with ChIP-seq analysis, this protocol may fail to clone DNA fragments due to the persistence of the TOP2β-phosphotyrosyl linkage created by etoposide treatment (see STAR Methods). Loss of these fragments may explain some differences in TOP2β gene body signal between eTIP experiments with different etoposide concentrations, as well as TOP2β ChIP-seq. Thus, while our findings provide insights into the activity of TOP2β, they may not present an exhaustive analysis of enzyme sites of action in neurons.

STAR★METHODS

RESOURCE AVAILABILITY

Lead contact—Further information and requests for reagents and resources should be directed toward the lead contact, Harrison W. Gabel (gabelh@wustl.edu).

Materials availability—Request for materials generated in this study should be directed toward the lead contact, Harrison W. Gabel (gabelh@wustl.edu).

Data and code availability

- All sequencing data have been deposited in the Gene Expression Omnibus (GEO) and are available under the accession number GSE246463 as of the date of publication. All mass spectrometry data have been deposited in the PRIDE database and are available under the accession number PXD046904 as of the date of publication.

- This paper does not report original code.
- Any additional information required to reanalyze the data reported in this paper is available from the lead contact upon request.

EXPERIMENTAL MODEL AND STUDY PARTICIPANT DETAILS

Mice—For mouse neuronal cortical cultures, embryonic day 14.5 (E14.5) male and female mouse embryos were prepared from adult C57BL/6J wild-type females. For eTIP from mouse brains, *MECP2* knockout mice (B6.129P2(C)-*MeCP2*tm1.Bird/J) and wild-type male littermates (*MeCP2*+/y) were obtained from The Jackson Laboratory at 8 weeks of age. All animal protocols were approved by the Institutional Animal Care and Use Committee (IACUC) and the Animal Studies Committee of Washington University in St. Louis, and in accordance with guidelines from the National Institutes of Health (NIH).

Mouse cortical cultures—Cortical neurons were cultured from C57BL/6J mouse embryos as described in,[5] with some modifications. E14.5 mouse cortices were dissected in 1X DPBS, dissociated and trypsinized with TrypLE Express for two 6 min incubations at 37°C, followed by DNAse treatment, to remove free-floating DNA and digest DNA from dead cells. Trituration of cells was performed with a pipette to dissociate cells fully. Dissociated neurons were seeded onto 6-well plates pre-coated with poly-D-lysine (0.1 mg/mL) at a density of 7.5×10^5 cells per well (or at a density of 3×10^5 cells per well for 12-well plates). The plates were pre-coated with poly-D-lysine (0.1 mg/mL) in water, washed three times with water and washed once with neurobasal medium before use. Neurons were cultured with neurobasal medium with 5% fetal bovine serum, GlutaMAX, B27 Supplement and Antibiotic-Antimycotic and maintained at 37°C with 5% CO_2. Neurons were grown *in vitro* for 3 days. At DIV3 and DIV9, cells were fed with one volume of neurobasal medium supplemented with 4.84 μg/mL uridine 5′-triphosphate, 2.46 μg/mL 5-fluoro-2′-deoxyuridine, GlutaMAX, B27 Supplement and Antibiotic-Antimycotic.

METHOD DETAILS

Mass spectrometry—Immunoprecipitation followed by mass spectrometry (IP-MS) was performed as previously described,[87,88] with modifications. Mouse DIV3 primary cortical neurons were infected with lentiviruses encoding FLAG-tagged baits under the CMV (IP1 in Figure 1; Table S1) or neuronal Synapsin1 (IP2 in Figure 1; Table S1) promoter. Each IP indicated in Figure 1 and Table S1 is the aggregate result from two independent IP mass-spec experiments per construct. Lysates of DIV10 cortical neurons were subjected to immunoprecipitation using FLAG resin (Sigma), followed by 3XFLAG peptide elution (Sigma) and trichloroacetic acid (TCA) precipitation.

Proteins were trypsinized (Sequencing-Grade Trypsin, Promega) and washed (3M Empore C18 media), and tryptic peptides were loaded onto an LTQ linear ion trap mass spectrometer (ThermoFinnigan). Spectra were searched against target-decoy tryptic peptide databases by ComPASS analysis. Weighted D-scores were generated by comparison of MeCP2 co-IP results to ComPASS analysis of a total of 18 bait proteins (data not shown).

Plasmids—The mouse TOP2β cDNA with a C-terminal MYC tag was amplified from MGC Mouse *Top2b* cDNA (Dharmacon) and cloned into pBACh, a modified pCAG (cytomegalovirus enhancer fused to chicken beta-actin promoter) vector, using restriction enzyme cloning at XhoI (5′) and NotI (3′). The modified pCAG vector was generated from a pCAG-mCherry, pIRES2-EGFP (Clontech) in which the IRES and EGFP were replaced by mCherry (a gift from Dr. Jason Yi). The truncated TOP2β constructs were generated by the insertion of PCR products into pBACh empty vector using Gibson Assembly cloning (NEB). All constructs were given consensus translation initiation sequences. Human full-length MeCP2 and MeCP2 fragments were cloned into p3xFLAG-CMV (a gift from Dr. Adrian Bird) and were the same as used previously.[36] Mouse full-length Dnmt3a was the same as used previously.[79] The MeCP2 shRNA and MeCP2 overexpression constructs were the same as used previously.[78]

Endogenous co-immunoprecipitation—Endogenous co-immunoprecipitations were carried out as described previously.[89] Forebrains from 8-week-old C57 B/J mice were isolated and lysed in NP-40 lysis buffer (10 mM HEPES, pH 7.9, 3 mM MgCl2, 10 mM KCl, 10 mM NaF, 1 mM Na3VO4, 0.5 mM DTT, 0.5% NP-40, 13 complete EDTA-free protease inhibitor cocktail (Roche)), dounced 15 times with a tight pestle, and pelleted at 1,000 g. Lysates were diluted 1:1 with benzonase buffer (10 mM HEPES, pH 7.9, 3 mM MgCl2, 280 mM NaCl, 0.2 mM EDTA, 10 mM NaF, 1 mM Na3VO4, 0.5 mM DTT, 0.5% NP-40, and 13 complete EDTA-free protease inhibitor cocktail (Roche)) and digested with 250 units benzonase (Millipore) for 1 h rotating at 4°C to release MeCP2 and its protein binding partners from the genome. Digested lysates were pelleted at 16,000 g for 20 min at 4°C and immunoprecipitation was carried out on the supernatant using the following antibodies: MeCP2 (07–013, Millipore) or TOP2β (H-286, sc-13059, Santa Cruz), in the presence of 150 mM NaCl for 2 h while rotating at 4°C. The peptide-block control lysate was immunoprecipitated with MeCP2 antibody in the presence of a peptide to which the antibody was raised.

Heterologous cell co-immunoprecipitation—HEK293T cells were transfected with TOP2β, MeCP2 or DNMT3A constructs using Lipofectamine 2000 (Invitrogen) and harvested after 24–48 h. HEK293T cells were lysed in NE10 buffer (20 mM HEPES (pH 7.5), 10 mM KCl, 1 mM MgCl2, 0.1% Triton X-100 (v/v), protease inhibitors (Roche), 15 mM β-mercaptoethanol), dounced 15 times and pelleted 5 min at 500 g. Nuclei were washed in NE10 buffer and then digested with 250 units benzonase (Millipore) for 30 min rotating at 25°C. Nuclei were resuspended in NE150 buffer (NE10 supplemented with 150mM NaCl) and incubated for 20 min. Lysates were pelleted at 16,000 g for 20 min at 4°C and supernatants were immunoprecipitated by incubating the Myc tag (ab9106, Abcam) antibody with Dynabeads Protein for 1 h at 4°C. The IP fraction was recovered by magnetic separation followed by three washes with NE10 buffer containing 150 mM-300 mM NaCl. The IP was then eluted from the beads with 2X NuPage LDS buffer (Invitrogen) containing β-mercaptoethanol.

Immunoblotting—Nuclear extracts or IP eluates from brain tissues or HEK293T cells were resolved on 5–12% Tris-Glycine gels and transferred to nitrocellulose. Membranes

were incubated overnight in the following primary antibodies: MeCP2 (Men-8, M7443, Sigma), TOP2β (H-286, sc-13059, Santa Cruz), TOP1 (H-5, sc-271285, Santa Cruz), Myc tag (ab9132, Abcam), FLAG tag (F3165, Sigma), α-Tubulin (EP1332Y, ab52866, Abcam). Following washes, membranes were incubated with HRP-conjugated secondary antibodies and visualized by enhanced chemiluminescence (ECL, Cell Signaling Technology) or secondary antibodies conjugated to IRdye 800 and imaged with LiCOR Odyssey.

RADAR assay—RADAR was performed as previously described.[63] HEK293T cells were transfected with full-length TOP2β-MYC and MeCP2-Flag constructs (as used in co-IP analysis) using Lipofectamine 2000 (Invitrogen) and harvested after 48–72 h. For cells transfected with and without TOP2β-MYC, GFP expressing plasmid was included to balance the total plasmid DNA transfected. On the day of harvest, cells were treated with either the vehicle (DMSO) or 0.5 mM etoposide for 15 min to capture TOP2β cleavage complexes. HEK293T cells were then lysed in DNAzol (Invitrogen)+1%Sarkosyl. DNA-protein complexes were pelleted by adding 100% ethanol to the lysates followed by centrifugation at 16,000 *g* for 15 min. The pellets were then washed with 75% ethanol for further purification and dissolved in 8mM NaOH at 4°C overnight. Samples were briefly sonicated and DNA was quantified. 200 ng of DNA was used for the slot blot. The membrane was washed and blotted with an anti-MYC antibody (ab9132, Abcam) followed by a secondary antibody conjugated to IRdye 800 and imaged with a LiCOR odyssey to detect TOP2β cleavage complexes. Signal for each sample was normalized by subtracting the signal in the vehicle condition and dividing by the TOP2β only condition. For Western blot analysis of protein expression, cells transfected in parallel were lysed directly in 2X NuPage LDS buffer (Invitrogen) and immunoblotted as described above.

Virus production—For lentiviral-mediated overexpression and shRNA knockdown of MeCP2, virus was prepared as described in[90] using the MeCP2 shRNA and MeCP2 overexpression plasmids previously validated in.[78] To produce lentivirus, 10 μg of lentiviral plasmid (either shRNA-expressing or MeCP2 overexpression) was transfected into HEK293T cells along with third generating packaging plasmids pMDL (5 μg), RSV (2.5 μg), and VSVG (2.5 μg). HEK293T cells were maintained in complete DMEM media (DMEM (high glucose) media, 10% fetal bovine serum, 1% GlutaMAX, 1% penicillin/streptomycin). At 12–16 h following transfection, media was replaced with fresh complete DMEM media. Viruses were concentrated by ultracentrifugation 48–60 h after transfection and viral titers were determined by infection of HEK293T cells and were typically 0.5–1×10^5 IFU/μL. Cultured neurons were infected on DIV3 and harvested on DIV12 for eTIP-seq, ChIP-seq or RNA-seq. In RNA-seq of neurons in which MeCP2 was not manipulated, cells were transduced with control virus that does not express a functional protein or shRNA to control for viral infection and facilitate better comparison to cells with lentiviral-mediated manipulations.

Etoposide-mediated topoisomerase immunoprecipitation (eTIP) protocol—eTIP experiments were performed as previously described,[66] with some modifications. E14.5 primary neuronal cultures were maintained for 12 days *in vitro* (DIV12) and then treated with 0.5 mM etoposide (VP-16) or DMSO control in serum-free medium for 15

min. The 2.1×10^6 treated cells were lysed with 300 μL of TE buffer (10 mM Tris and 1 mM EDTA, pH 8.0) and 1% SDS. Before sonication, 3 volumes of a buffer containing TE buffer and protease inhibitor (Complete Mini Roche) was added to the lysates. 5% of the lysates was saved for protein evaluation. To fragment DNA, the lysates were sonicated with Covaris E220 sonicator (5% Duty Factory, 140 Peak Incidence Power, 200 cycles per burst, milliTUBE 1mL AFA Fiber). Under these conditions, length of DNA fragments, as determined by TapeStation, varied from 0.5kb to 1.2kb. Before immunoprecipitation (IP), 3 volumes of a buffer containing 20 mM Tris-HCl (pH 8.0), 3% Triton X-100, 450mM NaCl, 3mM EDTA and protease inhibitor mixture was added to 1 volume of lysates. Because we utilized a conservative sonication protocol to avoid damaging TOP2β-DNA linkages, the average fragment length in our sequencing analysis was estimated to be 500bp-1000bp, leading to broader peaks than sometimes observed in genomic profiling approaches that result in smaller fragments (e.g., Cut&Tag).

The immunoprecipitation was carried out as previously described,[91] with some modifications. The diluted lysates were precleared with 15μL of Dynabeads Protein A by rotating the tubes for 2 h at 4°C. After pre-clear, 3% of the lysate was saved and used as input for the IP reaction. The unbound fraction was recovered by magnetic separation. The reaction was initiated by the addition of 15μL of Dynabeads Protein A, which was pre-incubated with 2 μg ofa TOP2β specific antibody. The beads suspension was incubated overnight at 4°C and the IP fraction was recovered by magnetic separation followed by two washes with low salt buffer (0.1% SDS, 1% Triton X-100, 2 mM EDTA, 20 mM Tris-HCl (pH 8.0), 150 mM NaCl), two washes with high salt buffer (0.1% SDS, 1% Triton X-100, 2 mM EDTA, 20 mM Tris- HCl (pH 8.0), 500 mM NaCl), two washes with LiCl buffer (0.250 mM LiCl, 1% NP40, 1% deoxycholic acid (sodium salt), 1 mM EDTA, 10 mM Tris (pH 8.0)) and one wash with TE buffer. The IP was then eluted from the beads twice by adding elution buffer containing TE buffer and 1% SDS and incubating the samples at 65°C for 30 min with brief vortexing every 10min. Elution buffer (1.5 volumes) was also added to the saved input material and this sample was processed together with the IP samples. Each eluate was treated with 10 μg RNAse A and incubated for 1 h at 37°C and then with 20 mg/mL Proteinase K and incubated for 2 h for 55°C. The IP DNA fragments were extracted with Phenol:Chloroform:Isoamyl alcohol (25:24:1, v/v). The resulting genomic DNA fragments were then purified using the QIAquick PCR purification kit (Qiagen) and DNA fragments were eluted from the columns twice.

Libraries were generated using ACCEL-NGS 2S PLUS DNA Library Kit (21024, Swift Biosciences), according to the manufacturer's instructions and PCR amplified for 12–16 cycles. Library quality was assessed using the Agilent 4200 TapeStation (Agilent Technologies). Libraries were pooled to a final concentration of 4–10 nM and 50bp reads were generated on the Illumina HiSeq 3000 with the Genome Technology Access Center, or 75bp reads were generated on the Illumina Nextseq 500 with the Center for Genome Science at Washington University in St. Louis, typically yielding 15–40 million single-end reads per sample. One potential issue with our library cloning procedure is the potential for TOP2β cleavage complexes (TOP2βcc), which will be covalently linked to the end of the DNA during pulldown to block the successful cloning of the DNA by ligation of adapters and PCR. We believe the proteinase K treatment and end-polishing steps in the DNA purification

and library cloning protocols likely remove this impediment and result in successful cloning of etoposide-linked TOP2β-cc fragments because we do not get sequencable libraries from samples in which etoposide is not included. However, it is possible that some TOP2βcc fragments failed to be capture in this procedure.

eTIP-seq from mouse brain—eTIP experiments were carried out on acute cortical slices obtained from 8-week-old *MeCP2* KO and wild-type male mice as previously described,[92] and in accordance with the Washington University in St Louis Animal Welfare Assurance D16-00245 and IACUC protocol 21–0372 (Papouin lab). Briefly, once deeply anesthetized with saturating amounts of isoflurane, mice were rapidly decapitated, and the brain was quickly removed in ice-cold artificial cerebrospinal fluid (aCSF) containing (in mM): 125 NaCl, 3.2 KCl, 1.25 NaH_2PO_4, 26 $NaHCO_3$, and 10 glucose (pH 7.3, 290-300mOsm.L^{-1}). aCSF was equilibrated with 95% O_2/5% CO_2 and containing 2mM Mg^{2+} and 1mM Ca^{2+} to minimize excitotoxicity. The aCSF composition Coronal slices (350μm) were obtained, cut into hemi-slices down the midline, and subcortical structures were removed. Cortical slices (n = 14–16 per mouse per genotype) were rested on nets that were submerged in aCSF saturated with 95% O_2/5% CO_2 containing 1.5mM Mg^{2+} and 2mM Ca^{2+} and incubated for 10 min at 33°C. Next, the slices were allowed to recover at room temperature for 30 min. The slices were then transferred into aCSF saturated with 95% O_2/5% CO_2, containing 1.5mM Mg^{2+} and 2mM Ca^{2+} at 37°C and 500μM etoposide (Santa Cruz, sc-3512a) for 15 min, with sister hemi-slices each assigned to a different experimental group: vehicle (DMSO) or treatment (DMSO + etoposide). Slices were then removed from aCSF and immediately prepared for eTIP-seq as described for cultured cortical neurons. Notably, as described for cultured neurons, DMSO-only treated brain slices did not yield quantifiable quantities of DNA and could not be cloned for sequencing, demonstrating the high specificity of the assay.

Chromatin immunoprecipitation protocol and library preparation (ChIP-seq)—ChIP experiments were performed on 2.1×10^6 mouse cortical neurons cultured to *in vitro* day 12 as described in,[91] with some modifications. To cross-link protein-DNA complexes, media was removed from primary neurons and cross-linking buffer (20 mM HEPES-NaOH, pH 8.0, 200mM NaCl, 2 mM EDTA, 2mM EGTA) containing 1% paraformaldehyde was added for 10 min at room temperature. Cross-linking was quenched by adding 125 mM glycine for 5 min at room temperature. Cells were then rinsed 2 times in ice-cold PBS containing PMSF protease inhibitor (Thermo Fisher) and collected by scrapping. Cells were lysed and nuclei isolated by incubating in L1 buffer (100 mM HEPES- NaOH, pH 7.5, 280 mM NaCl, 2 mM EDTA, 2mM EGTA, 0.5% Triton X-100, 1% NP-40, 20% Glycerol, 10 mM sodium butyrate, protease inhibitor cocktail (Roche)) for 10 min at 4°C. Nuclei were then pelleted by centrifugation at for 10 min at 4°C. The isolated nuclei were resuspended in L2 buffer (100 mM Tris-HCl, pH 8.0, 200 mM NaCl, 10 mM sodium butyrate, protease inhibitor cocktail (Roche)) and re-pelleted. The isolated nuclei were resuspended in L3 buffer (20 mM Tris-HCl, pH 8.0, 2 mM EDTA, 2mM EGTA, 10 mM sodium butyrate, protease inhibitor cocktail (Roche)). Nuclei were pelleted and either stored at −80°C until use or immediately processed. Chromatin was sonicated using a Bioruptor (Diagenode) on high power mode for 50 cycles with 30 s pulses in sonication buffer (20mM Tris-HCl, pH

8.0, 2 mM EDTA, 2mM EGTA, 10 mM sodium butyrate, 0.1% Na-Deoxycholate, 0.5% SDS, protease inhibitor cocktail (Roche)).

Following sonication, the immunoprecipitation was carried out as described for eTIP and the chromatin was incubated overnight at 4°C with H3K27ac (0.025–0.1 μg, Abcam 4729) or TOP2β (1–2 μg, Bethyl Laboratories A300-950A) and Protein A Dynabeads. H3K27ac and TOP2β ChIPs were performed twice from independent neuronal cultures. Following the overnight incubation, the IP was washed and eluted as described for eTIP. Libraries were generated using Ovation Ultralow Library System V2 (Tecan, 0344NB-32), according to the manufacturer's instructions and PCR amplified for 12–16 cycles. Library quality was assessed using the Agilent 4200 TapeStation (Agilent Technologies). Libraries were pooled to a final concentration of 4-10nM and 75bp reads were generated on the Illumina Nextseq 500 with the Center for Genome Science at Washington University in St. Louis, typically yielding 15–40 million single-end reads per sample.

Total RNA isolation and library preparation (RNA-seq)—Neuronal cultures dissected and transduced (with MeCP2 KD, MeCP2 OE or control virus) on the same days, constituted technical replicates, whereas, Neuronal cultures dissected and transduced on independent days, constituted biological replicates. Cultured neurons were harvested directly using RLT buffer and homogenized in the QIAshredder spin column (Qiagen). To isolate RNA, the RNeasy Mini Kit (Qiagen) according to the manufacturer's instructions. RNA libraries were generated from 250ng total RNA with rRNA depletion (NEBNext, E6310) and NEBNext Ultra Directional RNA Library Prep Kit for Illumina (NEBNext, E7420), using a modified amplification protocol (37°C, 15 min; 98°C, 30 s; (98°C, 10 s; 65°C, 30 s; 72°C, 30 s) x 13 cycles; 72°C, 5 min; 4°C, hold). RNA libraries were pooled at a final concentration of 8-10nM and single end 75bp reads were generated on the Illumina Nextseq 500 with the Center for Genome Science at Washington University in St. Louis, typically yielding 20–40 million single-end reads per sample.

QUANTIFICATION AND STATISTICAL ANALYSIS

Statistical methods and the numbers of biological replicates tested are presented in the figure legends. For comparisons between two groups, Fisher's exact tests or Wilcoxon rank-sum test were used as indicated in the figure legends. Statistical analysis was defined as n.s., not significant; *, $p < 0.05$; **, $p < 0.01$; ***, $p < 0.001$; ****, $p < 0.0001$; ‡,$p< 10^{-9}$; ‡‡,$p< 10^{-15}$. All data are presented as means mean ± SEM unless stated otherwise.

Etoposide-mediated topoisomerase immunoprecipitation sequencing analysis —eTIP-seq was analyzed as previously described for ChIP-seq data.[40] Sequenced reads were mapped to the mm9 genome using bowtie2 alignment and reads were extended based on library sizes and deduplicated to consolidate PCR duplicate reads.[82,84] Deduplicated reads were used to quantify read density normalized by the number of reads per sample and by read length in basepairs. Bedtools coverage -counts parameter was used to quantify eTIP signal and ChIP signal.[83]

For eTIP, the signal was quantified at promoter associated region, defined as 1kb downstream to 3kb downstream of the TSS, and the gene body, defined as 3kb downstream

of the TSS to the end of the transcript, based on our Ensembl gene models. edgeR[81] was then used to determine differential eTIP-signal across conditions. Data were visualized using UCSC genome browser (http://genome.ucsc.edu).

Aggregate plots of eTIP signal at genes and enhancers were generated by calculating eTIP/Input for equally sized bins for the specified windows using Bedtools coverage -hist parameter and custom R and Python scripts. For aggregate analysis at genes, the genes less than 3kb in length were filtered out in order to capture the signal at the promoter associated regions without conflating the ends of genes with this region. In some instances, the genes are further filtered such that the lengths of the genes plotted is equal to or greater than the aggregate length being plotted.[40]

Resampling control analysis was performed with custom scripts, by moving true TOP2β peak randomly around the genome with the criteria that the shuffled peaks do not overlap each other however could at random overlap a true TOP2β peak.

Chromatin immunoprecipitation sequencing analysis—ChIP-seq analysis was performed as previously described.[40] Sequenced reads were mapped to the mm9 genome using bowtie2 alignment and reads were extended based on library sizes and deduplicated to consolidate PCR duplicate reads. Deduplicated reads were used to quantify read density normalized by the number of reads per sample and by read length in base pairs. Bedtools coverage -counts parameter was used to quantify ChIP signal.

For H3K27ac ChIP, the signal was quantified at the TSS and enhancers. Enhancers in this study were defined by requiring the presence of H3K27ac peaks that occur outside of a known TSS region (TSS +/− 500bp). H3K27ac peaks were identified using MACS2 peak calling algorithm,[86] in which the ChIP input was used as background signal, using the following parameters: macs2 call peak –nomodal -q 0.05. Bedtools intersect was used to identify H3K27ac peaks that did not overlap with gene promoter regions. These filtered H3K27ac peaks were defined as enhancers. As noted, this may have led to the exclusion of some subthreshold regions of H3K27ac enrichment that may represent true regulatory elements.

For TOP2β ChIP, the signal was quantified as described for eTIP analysis. edgeR was used to determine differential ChIP signal across conditions.

RNA sequencing analysis—RNA sequencing analysis was performed as previously described.[40] Raw FASTQ files were trimmed with Trim Galore, using a quality filter of 20, followed by filtering out rRNA sequences using Bowtie2. The remaining reads were aligned to mm9 using STAR[85] with default parameters. Reads mapping to multiple regions in the genome were then filtered out, and uniquely mapped reads were converted to BED files and separated into intronic and exonic reads. Finally, reads were assigned to genes using bedtools coverage -counts parameter.[83]

For gene annotations, we defined a “flattened” list of the longest transcript for each gene, generated on Ensgene annotations and obtained from the UCSC table browser. For each gene, Ensembl IDs were matched up to the MGI gene names. Then, for each unique MGI

gene name, the most upstream Ensgene TSS and the most downstream TES were taken as the gene's start and stop. Based on these Ensembl gene models, we defined TSS regions, TSS-adjacent regions, and gene bodies. DESeq2[80] was run using default parameters on exonic reads from MeCP2 KD and MeCP2 OE cultured neurons ($n = 8$ per condition), to identify differentially expressed genes. The threshold for calling statistical significance was a false discovery rate [FDR] < 0.1.

Supplementary Material

Refer to Web version on PubMed Central for supplementary material.

ACKNOWLEDGMENTS

We thank D. Wu, N. Hamagami, Gabel lab members, and J. Yi for genomic analysis and critical reading of the manuscript. We thank W. Harper, E. Bennett, J. Lydeard, and Harper lab members, as well as N. Litterman, L. Mejia, and Bonni lab members, for contributions on the mass spectrometry experiments. We thank the Center for Genome Sciences (CGS) and the Genome Technology Access Center (GTAC) at Washington University in St. Louis for sequencing. This work was supported by the Klingenstein-Simons Fellowship Fund (H.W.G.), NIMH R01MH117405 (H.W.G.), NINDS R01NS04102 (H.W.G. and A.B.), NIMH 1R01MH127163-01 (T.P.), DoD W911NF-21-1-0312 (T.P.), Brain & Behavior Research Foundation 28616 (T.P.), Whitehall Foundation 2020-08-35 (T.P.), and McDonnell Center for Cellular and Molecular Neurobiology award 22-3930-26275U (T.P.).

REFERENCES

1. Closser M, Guo Y, Wang P, Patel T, Jang S, Hammelman J, De Nooij JC, Kopunova R, Mazzoni EO, Ruan Y, et al. (2022). An expansion of the non-coding genome and its regulatory potential underlies vertebrate neuronal diversity. Neuron 110, 70–85.e6. [PubMed: 34727520]
2. Gabel HW, Kinde B, Stroud H, Gilbert CS, Harmin DA, Kastan NR, Hemberg M, Ebert DH, and Greenberg ME (2015). Disruption of DNA-methylation-dependent long gene repression in Rett syndrome. Nature 522, 89–93. [PubMed: 25762136]
3. Sugino K, Hempel CM, Okaty BW, Arnson HA, Kato S, Dani VS, and Nelson SB (2014). Cell-Type-Specific Repression by Methyl-CpG-Binding Protein 2 Is Biased toward Long Genes. J. Neurosci 34, 12877–12883. [PubMed: 25232122]
4. Zylka MJ, Simon JM, and Philpot BD (2015). Gene length matters in neurons. Neuron 86, 353–355. [PubMed: 25905808]
5. King IF, Yandava CN, Mabb AM, Hsiao JS, Huang HS, Pearson BL, Calabrese JM, Starmer J, Parker JS, Magnuson T, et al. (2013). Topoisomerases facilitate transcription of long genes linked to autism. Nature 501, 58–62. [PubMed: 23995680]
6. McCoy MJ, Paul AJ, Victor MB, Richner M, Gabel HW, Gong H, Yoo AS, and Ahn TH (2018). LONGO: An R package for interactive gene length dependent analysis for neuronal identity. Bioinformatics 34, i422–i428. [PubMed: 29950021]
7. McCoy MJ, and Fire AZ (2020). Intron and gene size expansion during nervous system evolution. BMC Genom 21, 360.
8. Mabb AM, Kullmann PHM, Twomey MA, Miriyala J, Philpot BD, and Zylka MJ (2014). Topoisomerase 1 inhibition reversibly impairs synaptic function. Proc. Natl. Acad. Sci. USA 111, 17290–17295. [PubMed: 25404338]
9. Feng W, Kawauchi D, Körkel-Qu H, Deng H, Serger E, Sieber L, Lieberman JA, Jimeno-González S, Lambo S, Hanna BS, et al. (2017). Chd7 is indispensable for mammalian brain development through activation of a neuronal differentiation programme. Nat. Commun 8, 14758. [PubMed: 28317875]
10. Corbett KD, and Berger JM (2004). Structure, molecular mechanisms, and evolutionary relationships in DNA topoisomerases. Annu. Rev. Biophys. Biomol. Struct 33, 95–118. [PubMed: 15139806]

11. Nitiss JL (2009). DNA topoisomerase II and its growing repertoire of biological functions. Nat. Rev. Cancer 9, 327–337. [PubMed: 19377505]
12. Roca J (2009). Topoisomerase II: A fitted mechanism for the chromatin landscape. Nucleic Acids Res 37, 721–730. [PubMed: 19059997]
13. Pommier Y, Sun Y, Huang SYN, and Nitiss JL (2016). Roles of eukaryotic topoisomerases in transcription, replication and genomic stability. Nat. Rev. Mol. Cell Biol 17, 703–721. [PubMed: 27649880]
14. Koster DA, Croquette V, Dekker C, Shuman S, and Dekker NH (2005). Friction and torque govern the relaxation of DNA supercoils by eukaryotic topoisomerase IB. Nature 434, 671–674. [PubMed: 15800630]
15. Stewart L, Redinbo MR, Qiu X, Hol WG, and Champoux JJ (1998). A model for the mechanism of human topoisomerase I. Science 279. 1534–154. [PubMed: 9488652]
16. Austin CA, and Marsh KL (1998). Eukaryotic DNA topoisomerase IIβ. Bioessays 20, 215–226. [PubMed: 9631649]
17. Austin CA, Sng JH, Patel S, and Fisher LM (1993). Novel HeLa topoisomerase II is the IIβ isoform: complete coding sequence and homology with other type II topoisomerases. Biochim. Biophys. Acta 1172, 283–291. [PubMed: 8383537]
18. Jenkins JR, Ayton P, Jones T, Davies SL, Simmons DL, Harris AL, Sheer D, and Hickson ID (1992). Isolation of cDNA clones encoding the b isozyme of human DNA topoisomerase II and localisation of the gene to chromosome 3p24. Nucleic Acids Res 20, 5587–5592. [PubMed: 1333583]
19. Tiwari VK, Burger L, Nikoletopoulou V, Deogracias R, Thakurela S, Wirbelauer C, Kaut J, Terranova R, Hoerner L, Mielke C, et al. (2012). Target genes of Topoisomerase IIβ regulate neuronal survival and are defined by their chromatin state. Proc. Natl. Acad. Sci. USA 109, E934–E943. [PubMed: 22474351]
20. Harkin LF, Gerrelli D, Gold Diaz DC, Santos C, Alzu'bi A, Austin CA, and Clowry GJ (2016). Distinct expression patterns for type II topoisomerases IIA and IIB in the early foetal human telencephalon. J. Anat 228, 452–463. [PubMed: 26612825]
21. Capranico G, Tinelli S, Austin CA, Fisher ML, and Zunino F (1992). Different patterns of gene expression of topoisomerase II isoforms in differentiated tissues during murine development. Biochim. Biophys. Acta 1132, 43–48. [PubMed: 1380833]
22. Watanabe M, Tsutsui K, Tsutsui K, and Inoue Y (1994). Differential expressions of the topoisomerase IIα and IIβ mRNAs in developing rat brain. Neurosci. Res 19, 51–57. [PubMed: 8008235]
23. Juenke JM, and Holden JA (1993). The distribution of DNA topoisomerase II isoforms in differentiated adult mouse tissues. Biochim. Biophys. Acta 1216, 191–196. [PubMed: 8241259]
24. Kondapi AK, Mulpuri N, Mandraju RK, Sasikaran B, and Subba Rao K (2004). Analysis of age dependent changes of Topoisomerase II a and b in rat brain. Int. J. Dev. Neurosci 22, 19–30. [PubMed: 15013075]
25. Tsutsui K, Tsutsui K, Okada S, Watanabe M, Shohmori T, Seki S, and Inoue Y (1993). Molecular cloning of partial cDNAs for rat DNA topoisomerase II isoforms and their differential expression in brain development. J. Biol. Chem 268, 19076–19083. [PubMed: 8395528]
26. Yang X, Li W, Prescott ED, Burden SJ, and Wang JC (2000). DNA topoisomerase IIβ and neural development. Science 287, 131–134. [PubMed: 10615047]
27. Lyu YL, and Wang JC (2003). Aberrant lamination in the cerebral cortex of mouse embryos lacking DNA topoisomerase IIβ. Proc. Natl. Acad. Sci. USA 100, 7123–7128. [PubMed: 12773624]
28. Ju BG, Lunyak VV, Perissi V, Garcia-Bassets I, Rose DW, Glass CK, and Rosenfeld MG (2006). A topoisomerase IIβ-mediated dsDNA break required for regulated transcription. Science 312, 1798–1802. [PubMed: 16794079]
29. Lyu YL, Lin C-P, Azarova AM, Cai L, Wang JC, and Liu LF (2006). Role of Topoisomerase IIβ in the Expression of Developmentally RegulatedGenes. Mol. Cell Biol 26, 7929–7941. [PubMed: 16923961]

30. Renthal W, Boxer LD, Hrvatin S, Li E, Silberfeld A, Nagy MA, Griffith EC, Vierbuchen T, and Greenberg ME (2018). Characterization of human mosaic Rett syndrome brain tissue by single-nucleus RNA sequencing. Nat. Neurosci 21, 1670–1679. [PubMed: 30455458]

31. Boxer LD, Renthal W, Greben AW, Whitwam T, Silberfeld A, Stroud H, Li E, Yang MG, Kinde B, Griffith EC, et al. (2020). MeCP2 Represses the Rate of Transcriptional Initiation of Highly Methylated Long Genes. Mol. Cell 77, 294–309.e9. [PubMed: 31784358]

32. Chen L, Chen K, Lavery LA, Baker SA, Shaw CA, Li W, and Zoghbi HY (2015). MeCP2 binds to non-CG methylated DNA as neurons mature, influencing transcription and the timing of onset for Rett syndrome. Proc. Natl. Acad. Sci. USA 112, 5509–5514. [PubMed: 25870282]

33. Lagger S, Connelly JC, Schweikert G, Webb S, Selfridge J, Ramsahoye BH, Yu M, He C, Sanguinetti G, Sowers LC, et al. (2017). MeCP2 recognizes cytosine methylated tri-nucleotide and di-nucleotide sequences to tune transcription in the mammalian brain. PLoS Genet 13, e1006793. [PubMed: 28498846]

34. Amir RE, Van Den Veyver IB, Wan M, Tran CQ, Francke U, and Zoghbi HY (1999). Rett syndrome is caused by mutations in X-linked MECP2, encoding methyl- CpG-binding protein 2. Nat. Genet 23, 185–188. [PubMed: 10508514]

35. Van Esch H, Bauters M, Ignatius J, Jansen M, Raynaud M, Hollanders K, Lugtenberg D, Bienvenu T, Jensen LR, Gécz J, et al. (2005). Duplication of the MECP2 region is a frequent cause of severe mental retardation and progressive neurological symptoms in males. Am. J. Hum. Genet 77, 442–453. [PubMed: 16080119]

36. Lyst MJ, Ekiert R, Ebert DH, Merusi C, Nowak J, Selfridge J, Guy J, Kastan NR, Robinson ND, De Lima Alves F, et al. (2013). Rett syndrome mutations abolish the interaction of MeCP2 with the NCoR/SMRT co-repressor. Nat. Neurosci 16, 898–902. [PubMed: 23770565]

37. Nan X, Meehan RR, and Bird A (1993). Dissection of the methyl-CpG binding domain from the chromosomal protein MeCP2. Nucleic Acids Res 21, 4886–4892. [PubMed: 8177735]

38. Chahrour M, Sung YJ, Shaw C, Zhou X, Wong STC, Qin J, and Zoghbi HY (2008). MeCP2, a key contributor to neurological disease, activates and represses transcription. Science, 320.

39. Lewis JD, Meehan RR, Henzel WJ, Maurer-Fogy I, Jeppesen P, Klein F, and Bird A (1992). Purification, sequence, and cellular localization of a novel chromosomal protein that binds to Methylated DNA. Cell 69, 905–914. [PubMed: 1606614]

40. Clemens AW, Wu DY, Moore JR, Christian DL, Zhao G, and Gabel HW (2020). MeCP2 Represses Enhancers through Chromosome Topology-Associated DNA Methylation. Mol. Cell 77, 279–293.e8. [PubMed: 31784360]

41. Zhou J, Hamdan H, Yalamanchili HK, Pang K, Pohodich AE, Lopez J, Shao Y, Oses-Prieto JA, Li L, Kim W, et al. (2022). Disruption of MeCP2–TCF20 complex underlies distinct neurodevelopmental disorders. Proc. Natl. Acad. Sci. USA 119. e2119078119. [PubMed: 35074918]

42. Li R, Dong Q, Yuan X, Zeng X, Gao Y, Chiao C, Li H, Zhao X, Keles S, Wang Z, and Chang Q (2016). Misregulation of Alternative Splicing in a Mouse Model of Rett Syndrome. PLoS Genet 12, e1006129. [PubMed: 27352031]

43. Baker SA, Lombardi LM, and Zoghbi HY (2015). Karyopherin a 3 and karyopherin a 4 proteins mediate the nuclear import of Methyl-CpG binding protein 2. J. Biol. Chem 290, 22485–22493. [PubMed: 26245896]

44. Leoh LS, Van Heertum B, De Rijck J, Filippova M, Rios-Colon L, Basu A, Martinez SR, Tungteakkhun SS, Filippov V, Christ F, et al. (2012). The stress oncoprotein LEDGF/p75 interacts with the methyl CpG binding protein MeCP2 and influences its transcriptional activity. Mol. Cancer Res 10, 378–391. [PubMed: 22275515]

45. Alomaim MM, and Mushiba AM (2023). A Novel De Novo Mutation of the DHX30 Gene in a Patient With Neurodevelopmental Disorder, Severe Motor Impairment, and Absent Language (NEDMIAL). Cureus 15, e33682. [PubMed: 36643085]

46. Mannucci I, Dang NDP, Huber H, Murry JB, Abramson J, Althoff T, Banka S, Baynam G, Bearden D, Beleza-Meireles A, et al. (2021). Genotype–phenotype correlations and novel molecular insights into the DHX30-associated neurodevelopmental disorders. Genome Med 13, 90. [PubMed: 34020708]

47. Heckman LD, Chahrour MH, and Zoghbi HY (2014). Rett-causing mutations reveal two domains critical for MeCP2 function and for toxicity in MECP2 duplication syndrome mice. Elife 3, e02676. [PubMed: 24970834]
48. Baker SA, Chen L, Wilkins AD, Yu P, Lichtarge O, and Zoghbi HY (2013). An AT-Hook Domain in MeCP2 Determines the Clinical Course of Rett Syndrome and Related Disorders. Cell 152, 984–996. [PubMed: 23452848]
49. Wang JC (1996). DNA topoisomerases. Annu. Rev. Biochem 65, 635–692. [PubMed: 8811192]
50. Watt PM, and Hickson ID (1994). Structure and function of type II DNA topoisomerases. Biochem. J 303, 681–695. [PubMed: 7980433]
51. Caron PR, and Wang JC (1994). Appendix II: Alignment of Primary Sequences of DNA Topoisomerases. Adv. Pharmacol 29B, 271–297. [PubMed: 8996613]
52. Austin CA, Marsh KL, Wasserman RA, Willmore E, Sayer PJ, Wang JC, and Fisher LM (1995). Expression, domain structure, and enzymatic properties of an active recombinant human DNA topoisomerase IIβ. J. Biol. Chem 270, 15739–15746. [PubMed: 7797575]
53. Lindsley JE, and Wang JC (1991). Proteolysis patterns of epitopically labeled yeast DNA topoisomerase II suggest an allosteric transition in the enzyme induced by ATP binding. Proc. Natl. Acad. Sci. USA 88, 10485–10489. [PubMed: 1720543]
54. Berger JM, Gamblin SJ, Harrison SC, and Wang JC (1996). Structure and mechanism of DNA topoisomerase II. Nature 379, 225–232. [PubMed: 8538787]
55. Chang CC, Wang YR, Chen SF, Wu CC, and Chan NL (2013). New insights into DNA-binding by type IIA topoisomerases. Curr. Opin. Struct. Biol 23, 125–133. [PubMed: 23265999]
56. Chen SH, Chan NL, and Hsieh TS (2013). New mechanistic and functional insights into DNA topoisomerases. Annu. Rev. Biochem 82, 139–170. [PubMed: 23495937]
57. Linka RM, Porter ACG, Volkov A, Mielke C, Boege F, and Christensen MO (2007). C-Terminal regions of topoisomerase IIα and IIβ determine isoform-specific functioning of the enzymes in vivo. Nucleic Acids Res 35, 3810–3822. [PubMed: 17526531]
58. Meczes EL, Gilroy KL, West KL, and Austin CA (2008). The impact of the human DNA topoisomerse II C-terminal domain on activity. PLoS One 3, e1754. [PubMed: 18335031]
59. Gilroy KL, and Austin CA (2011). The impact of the C-Terminal domain on the interaction of human DNA topoisomerase II a and b with DNA. PLoS One 6, e14693. [PubMed: 21358820]
60. Guo JU, Su Y, Shin JH, Shin J, Li H, Xie B, Zhong C, Hu S, Le T, Fan G, et al. (2014). Distribution, recognition and regulation of non-CpG methylation in the adult mammalian brain. Nat. Neurosci 17, 215–222. [PubMed: 24362762]
61. Lister R, Mukamel EA, Nery JR, Urich M, Puddifoot CA, Johnson ND, Lucero J, Huang Y, Dwork AJ, Schultz MD, et al. (2013). Global epigenomic reconfiguration during mammalian brain development. Science 341, 1237905. [PubMed: 23828890]
62. Tillotson R, Selfridge J, Koerner MV, Gadalla KKE, Guy J, De Sousa D, Hector RD, Cobb SR, and Bird A (2017). Radically truncated MeCP2 rescues Rett syndrome-like neurological defects. Nature 550, 398–401. [PubMed: 29019980]
63. Kiianitsa K, and Maizels N (2013). A rapid and sensitive assay for DNAprotein covalent complexes in living cells. Nucleic Acids Res 41, e104–e107. [PubMed: 23519618]
64. Osheroff N (1989). Effect of Antineoplastic Agents on the DNA Cleavage/Religation Reaction of Eukaryotic Topoisomerase II: Inhibition of DNA Re-ligation by Etoposide. Biochemistry 28, 6157–6160. [PubMed: 2551366]
65. Wu CC, Li TK, Farh L, Lin LY, Lin TS, Yu YJ, Yen TJ, Chiang CW, and Chan NL (2011). Structural basis of type II topoisomerase inhibition by the anticancer drug etoposide. Science 333, 459–462. [PubMed: 21778401]
66. Sano K, Miyaji-Yamaguchi M, Tsutsui KM, and Tsutsui K (2008). Topoisomerase IIβ activates a subset of neuronal genes that are repressed in AT-rich genomic environment. PLoS One 3, e4103. [PubMed: 19116664]
67. Skene PJ, Illingworth RS, Webb S, Kerr ARW, James KD, Turner DJ, Andrews R, and Bird AP (2010). Neuronal MeCP2 Is Expressed at Near Histone-Octamer Levels and Globally Alters the Chromatin State. Mol. Cell 37, 457–468. [PubMed: 20188665]

68. Balmer D, Goldstine J, Rao YM, and LaSalle JM (2003). Elevated methyl-CpG-binding protein 2 expression is acquired during postnatal human brain development and is correlated with alternative polyadenylation. J. Mol. Med 81, 61–68. [PubMed: 12545250]
69. Clemens AW, and Gabel HW (2020). Emerging Insights into the Distinctive Neuronal Methylome. Trends Genet 36, 816–832. [PubMed: 32839016]
70. Stroud H, Su SC, Hrvatin S, Greben AW, Renthal W, Boxer LD, Nagy MA, Hochbaum DR, Kinde B, Gabel HW, and Greenberg ME (2017). Early-Life Gene Expression in Neurons Modulates Lasting Epigenetic States. Cell 171, 1151–1164.e16. [PubMed: 29056337]
71. de Mendoza A, Poppe D, Buckberry S, Pflueger J, Albertin CB, Daish T, Bertrand S, de la Calle-Mustienes E, Gómez-Skarmeta JL, Nery JR, et al. (2021). The emergence of the brain non-CpG methylation system in vertebrates. Nat. Ecol. Evol 5, 369–378. [PubMed: 33462491]
72. Madabhushi R, Gao F, Pfenning AR, Pan L, Yamakawa S, Seo J, Rueda R, Phan TX, Yamakawa H, Pao PC, et al. (2015). Activity-Induced DNA Breaks Govern the Expression of Neuronal Early-Response Genes. Cell 161, 1592–1605. [PubMed: 26052046]
73. Lyst MJ, and Bird A (2015). Rett syndrome: A complex disorder with simple roots. Nat. Rev. Genet 16, 261–275. [PubMed: 25732612]
74. Kruusvee V, Lyst MJ, Taylor C, Tarnauskaitė Ž, Bird AP, and Cook AG (2017). Structure of the MeCP2-TBLR1 complex reveals a molecular basis for Rett syndrome and related disorders. Proc. Natl. Acad. Sci. USA 114, E3243–E3250. [PubMed: 28348241]
75. Wei PC, Chang AN, Kao J, Du Z, Meyers RM, Alt FW, and Schwer B (2016). Long Neural Genes Harbor Recurrent DNA Break Clusters in Neural Stem/Progenitor Cells. Cell 164, 644–655. [PubMed: 26871630]
76. Alessio N, Riccitiello F, Squillaro T, Capasso S, Del Gaudio S, Di Bernardo G, Cipollaro M, Melone MAB, Peluso G, and Galderisi U (2018). Neural stem cells from a mouse model of Rett syndrome are prone to senescence, show reduced capacity to cope with genotoxic stress, and are impaired in the differentiation process. Exp. Mol. Med 50, 1.
77. Enikanolaiye A, Ruston J, Zeng R, Taylor C, Schrock M, Buchovecky CM, Shendure J, Acar E, and Justice MJ (2020). Suppressor mutations in Mecp2-null mice implicate the DNA damage response in Rett syndrome pathology
78. Zhou Z, Hong EJ, Cohen S, Zhao WN, Ho HYH, Schmidt L, Chen WG, Lin Y, Savner E, Griffith EC, et al. (2006). Brain-Specific Phosphorylation of MeCP2 Regulates Activity-Dependent Bdnf Transcription, Dendritic Growth, and Spine Maturation. Neuron 52, 255–269. [PubMed: 17046689]
79. Christian DL, Wu DY, Martin JR, Moore JR, Liu YR, Clemens AW, Nettles SA, Kirkland NM, Papouin T, Hill CA, et al. (2020). DNMT3A Haploinsufficiency Results in Behavioral Deficits and Global Epigenomic Dysregulation Shared across Neurodevelopmental Disorders. Cell Rep 33, 108416. [PubMed: 33238114]
80. Love MI, Huber W, and Anders S (2014). Moderated estimation of fold change and dispersion for RNA-seq data with DESeq2. Genome Biol 15, 550. [PubMed: 25516281]
81. Robinson MD, McCarthy DJ, and Smyth GK (2010). edgeR: A Bioconductor package for differential expression analysis of digital gene expression data. Bioinformatics 26, 139–140. [PubMed: 19910308]
82. Li H, and Durbin R (2009). Fast and accurate short read alignment with Burrows-Wheeler transform. Bioinformatics 25, 1754–1760. [PubMed: 19451168]
83. Quinlan AR, and Hall IM (2010). BEDTools: A flexible suite of utilities for comparing genomic features. Bioinformatics 26, 841–842. [PubMed: 20110278]
84. Langmead B, and Salzberg SL (2012). Fast gapped-read alignment with Bowtie 2. Nat. Methods 9, 357–359. [PubMed: 22388286]
85. Dobin A, Davis CA, Schlesinger F, Drenkow J, Zaleski C, Jha S, Batut P, Chaisson M, and Gingeras TR (2013). STAR: Ultrafast universal RNA-seq aligner. Bioinformatics 29, 15–21. [PubMed: 23104886]
86. Zhang Y, Liu T, Meyer CA, Eeckhoute J, Johnson DS, Bernstein BE, Nusbaum C, Myers RM, Brown M, Li W, and Liu XS (2008). Model-based analysis of ChIP-Seq (MACS). Genome Biol 9, R137. [PubMed: 18798982]

87. Sowa ME, Bennett EJ, Gygi SP, and Harper JW (2009). Defining the Human Deubiquitinating Enzyme Interaction Landscape. Cell 138, 389–403. [PubMed: 19615732]

88. Mejia LA, Litterman N, Ikeuchi Y, de la Torre-Ubieta L, Bennett EJ, Zhang C, Harper JW, and Bonni A (2013). A Novel Hap1-Tsc1 interaction regulates neuronal mTORC1 signaling and morphogenesis in the brain. J. Neurosci 33, 18015–18021. [PubMed: 24227713]

89. Ebert DH, Gabel HW, Robinson ND, Kastan NR, Hu LS, Cohen S, Navarro AJ, Lyst MJ, Ekiert R, Bird AP, and Greenberg ME (2013). Activity-dependent phosphorylation of MeCP2 threonine 308 regulates interaction with NCoR. Nature 499, 341–345. [PubMed: 23770587]

90. Tiscornia G, Singer O, and Verma IM (2006). Production and purification of lentiviral vectors. Nat. Protoc 1, 241–245. [PubMed: 17406239]

91. Kim TK, Hemberg M, Gray JM, Costa AM, Bear DM, Wu J, Harmin DA, Laptewicz M, Barbara-Haley K, Kuersten S, et al. (2010). Widespread transcription at neuronal activity-regulated enhancers. Nature 465, 182–187. [PubMed: 20393465]

92. Papouin T, and Haydon PG (2018). Obtaining Acute Brain Slices. Bio. Protoc 8, e2699.

Highlights

- TOP2β is an MeCP2-interacting protein in neurons
- TOP2β activity is enriched at promoters and enhancers of long neuronal genes
- MeCP2 represses TOP2β activity at regulatory regions within MeCP2-regulated genes
- Loss of MeCP2 leads to hyperactivation of TOP2β in long genes regulated by MeCP2

A

	IP1		IP2		Mean	
Protein	TSC	WD-score	TSC	WD-score	TSC	WD-score
MeCP2	48	62.4	82	81.5	65	71.9
MTAP2	65	72.6	60	69.7	63	71.1
DHX30	10	28.5	11	29.9	11	29.2
JAKMIP1	15	34.9	6	22.1	11	28.5
CAMSAP3	6	22.1	10	28.5	8	25.3
TOP2B	**6**	**22.1**	**8**	**25.5**	**7**	**23.8**
SFRS14	6	22.1	6	22.1	6	22.1
SBF1	11	19.9	14	22.5	13	21.2
KPNA3	5	20.1	6	22.1	5.5	21.1
PSIP1	4	18.0	6	22.1	5	20.0

B

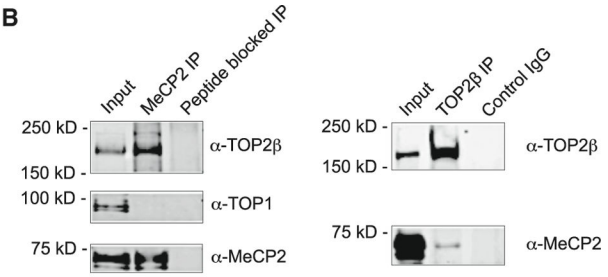

Figure 1. MeCP2 interacts with TOP2β in neurons

(A) Proteins co-immunoprecipitating (coIP) with immunoprecipitated (IP) FLAG-MeCP2 expressed under a lentivirus CMV (IP1) or Synapsin1 (IP2) promoter. Ten proteins are shown, with highest average weighted D scores detected by liquid chromatography-tandem mass spectrometry (LC/MS/MS) and ComPASS analysis in both IPs (see STAR Methods; Table S1). Spectral count and average weighted D (WD) scores are shown.

(B) Left, MeCP2 IP-western blot analysis from wild-type mouse forebrain nuclear extracts detects coIP of TOP2β but not TOP1. Right, IP of TOP2β showing coIP of MeCP2. Representative images, n = 2 biological replicates per coIP analysis. “Peptide blocked IP,” IP performed after pre-incubation of the antibody with peptide to which it was raised. “Control IgG,” IP with antibody against another protein, CtBP.

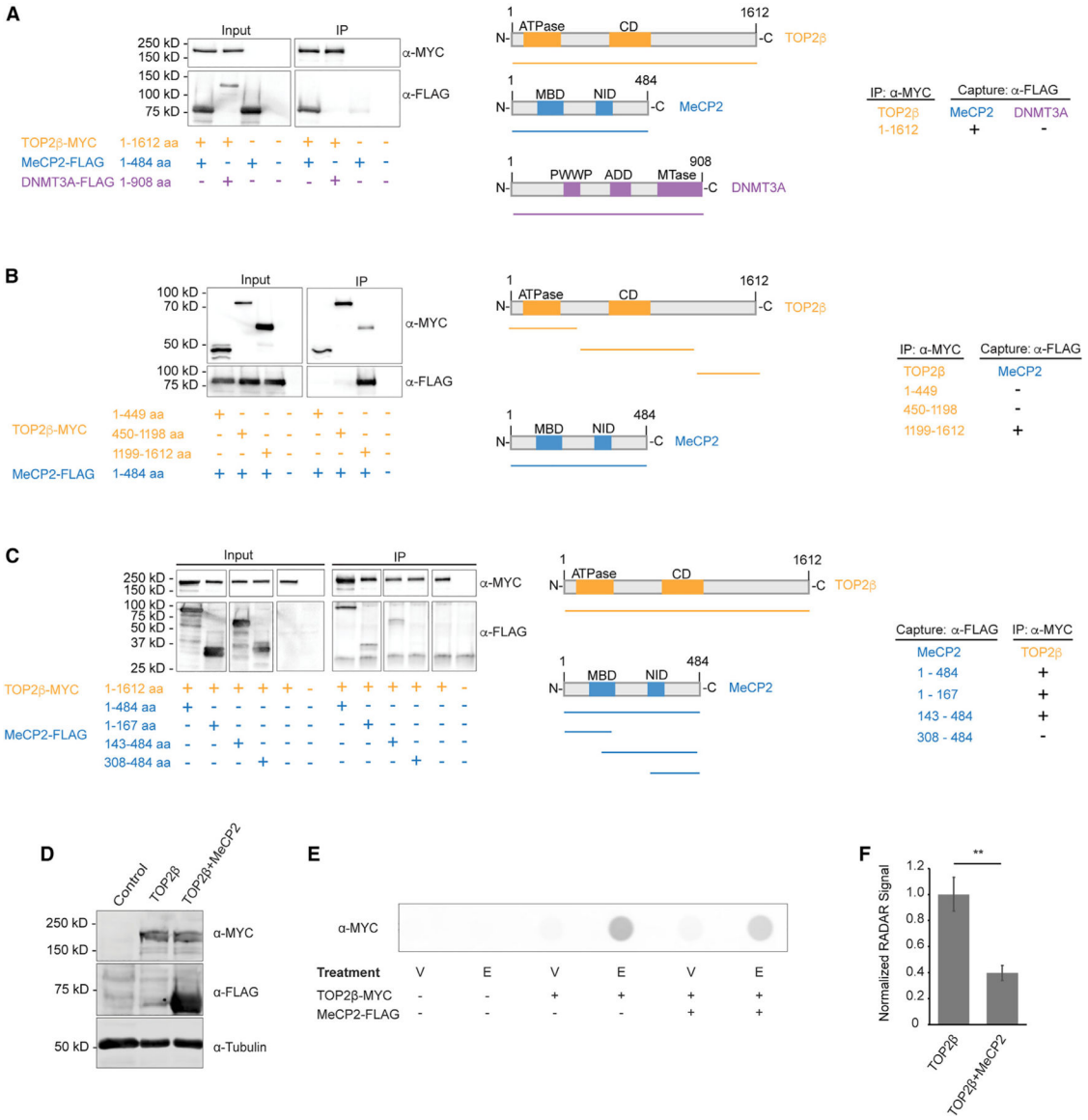

Figure 2. Mapping relevant protein domains and the functional impact of the MeCP2-TOP2β interaction

(A) Co-immunoprecipitation analysis of MYC-tagged full-length TOP2β, FLAG-tagged full-length MeCP2, and FLAG-tagged full-length DNMT3A in HEK293T cells. Left, western blot analysis of IP. Center, overview of protein domains. Right, results summary. CD, catalytic domain; MBD, methyl-DNA-binding domain; NID, NCoR-interaction domain; PWWP, proline-tryptophan-tryptophan-proline domain; ADD, ATRX-DNMT3A-DNMT3L domain; MTase, methyltransferase domain. Representative images (A) though (E) of at least two biological replicates.

(B) Co-immunoprecipitation analysis of MYC-tagged TOP2β fragments with full-length FLAG-tagged MeCP2 in HEK293T cells. As described in (A).

(C) Co-immunoprecipitation analysis of FLAG-tagged MeCP2 fragments with MYC-tagged full-length TOP2β. As described in (A).

(D) Western blot of protein lysates from transfected HEK293T cells used in RADAR analysis, showing the equal expression of MYC-tagged full-length TOP2β in the presence or absence of FLAG-tagged full-length MeCP2. α-tubulin was used as a control for protein loading.

(E) RADAR signal from HEK293T cells treated with vehicle (V) or etoposide (E). Increased RADAR signal is detected upon etoposide treatment in TOP2β-transfected conditions to capture TOP2β cleavage complexes trapped on the DNA. A decrease in RADAR signal was detected upon co-transfection of FLAG-tagged full-length MeCP2.

(F) Quantification of RADAR signal with and without co-expression of MeCP2 demonstrates MeCP2 inhibition of TOP2β cutting activity. Data shown are mean ± SEM. $^{**}p < 0.01$; n = 3 biological replicates.

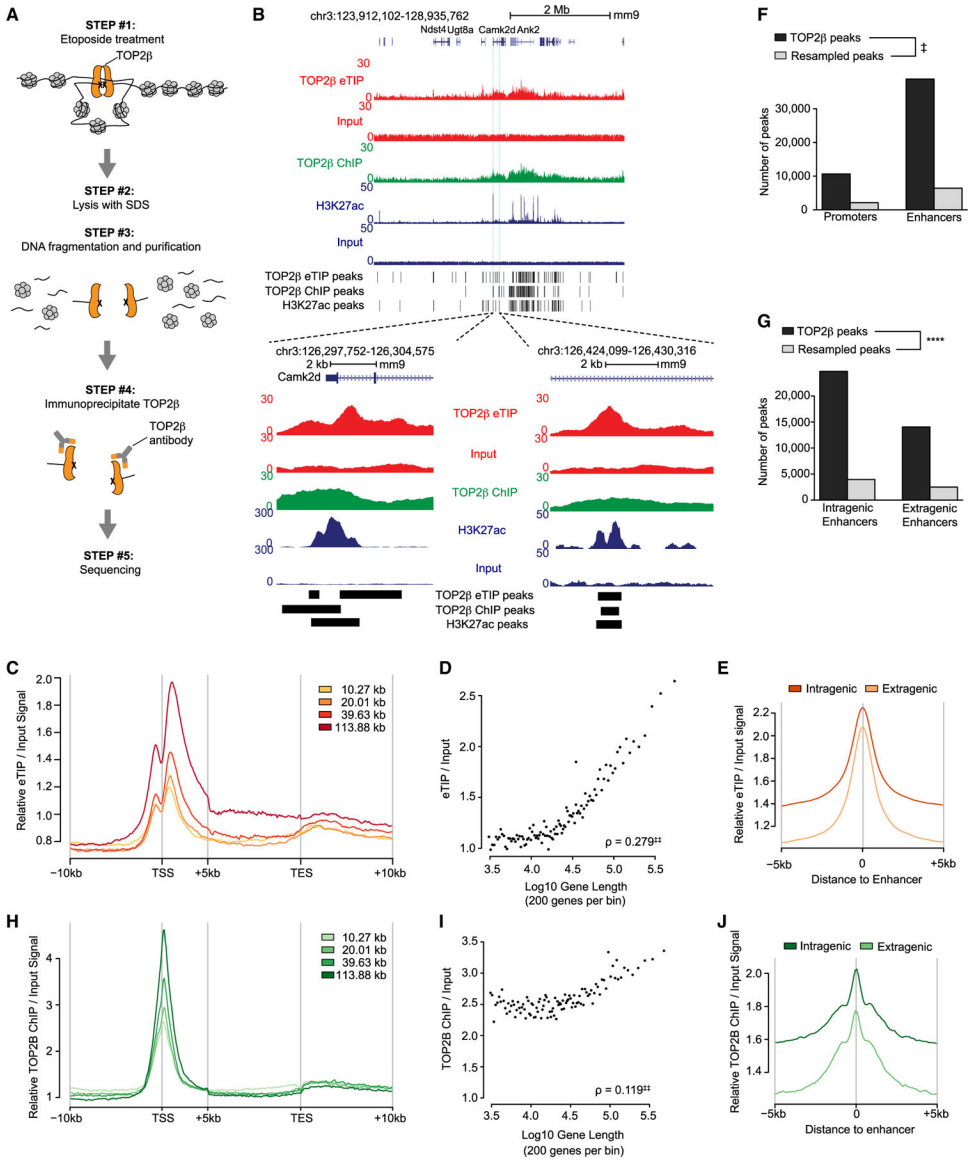

Figure 3. TOP2β is preferentially active at long genes in neurons

(A) Schematic representation of the eTIP-seq procedure to directly map sites of TOP2β activity.[66] TOP2β cleaves a DNA duplex to pass through a second DNA duplex and resolve constraints. In eTIP, etoposide treatment freezes TOP2β in its cleavage complex, covalently linked to its site of action. Following fragmentation under stringent purification, TOP2β-linked DNA is immunoprecipitated and sequenced.

(B) Genome browser tracks of eTIP-seq, as well as TOP2β and H3K27ac ChIP-seq, from DIV12 cultured neurons. Top, ~2 Mb region displaying profiles for TOP2β eTIP, TOP2β ChIP, H3K27ac, and inputs. Enrichment of eTIP-seq signal is prominent at long genes (e.g., *Camk2d*) compared with shorter genes (e.g., *Ugt8a*). Bottom, zoom-in views of *Camk2d* promoter and enhancer regions. Peaks of TOP2β eTIP, TOP2β ChIP, and H3K27ac ChIP called by MACS2 are indicated below the tracks. Data from DIV12 wild-type primary

neuron cultures. eTIP-seq, n = 4 biological replicates. TOP2β and H3K27ac ChIP-seq, n = 2 biological replicates.

(C) Aggregate plot of eTIP signal at genes divided into gene length quantiles (see STAR Methods). Median gene length for each quantile is indicated. TSS, transcription start site; TES, transcription end site; mean values plotted for 100 bp bins.

(D) Running average of eTIP signal at promoter-associated regions for 200 gene bins ranked by gene length. Spearman rho shown for gene length and eTIP signal. ‡‡$p < 10^{-15}$.

(E) Aggregate plot of eTIP signal at putative intragenic and extragenic enhancers genome wide in cultured neurons. Putative enhancers are defined as H3K27ac peaks that do not overlap a gene TSS. Plot is centered at the midpoint for each enhancer, mean values are plotted for 100 bp bins.

(F) Genomic distribution of TOP2β re-sampled control peaks at promoters and enhancers. Re-sampled peaks were generated by shuffling TOP2β peak-sized regions randomly around the genome (see STAR Methods). ‡$p < 10^{-9}$; chi-squared test, overlap of true TOP2β peaks vs. re-sampled TOP2β peaks.

(G) Genomic distribution of TOP2β and re-sampled control peaks at intragenic and extragenic enhancers. ****$p < 0.0001$, chi-squared test as in (F).

(H) Aggregate plot of TOP2β ChIP signal across gene length quantiles (see STAR Methods). Plotted as in (C).

(I) Running average plots of TOP2β ChIP signal at the promoter-associated regions of genes according to gene length. Correlation analysis as in (D). ‡‡$p< 10^{-15}$.

(J) Aggregate plot of TOP2β ChIP signal at enhancers. Plotted as in (E).

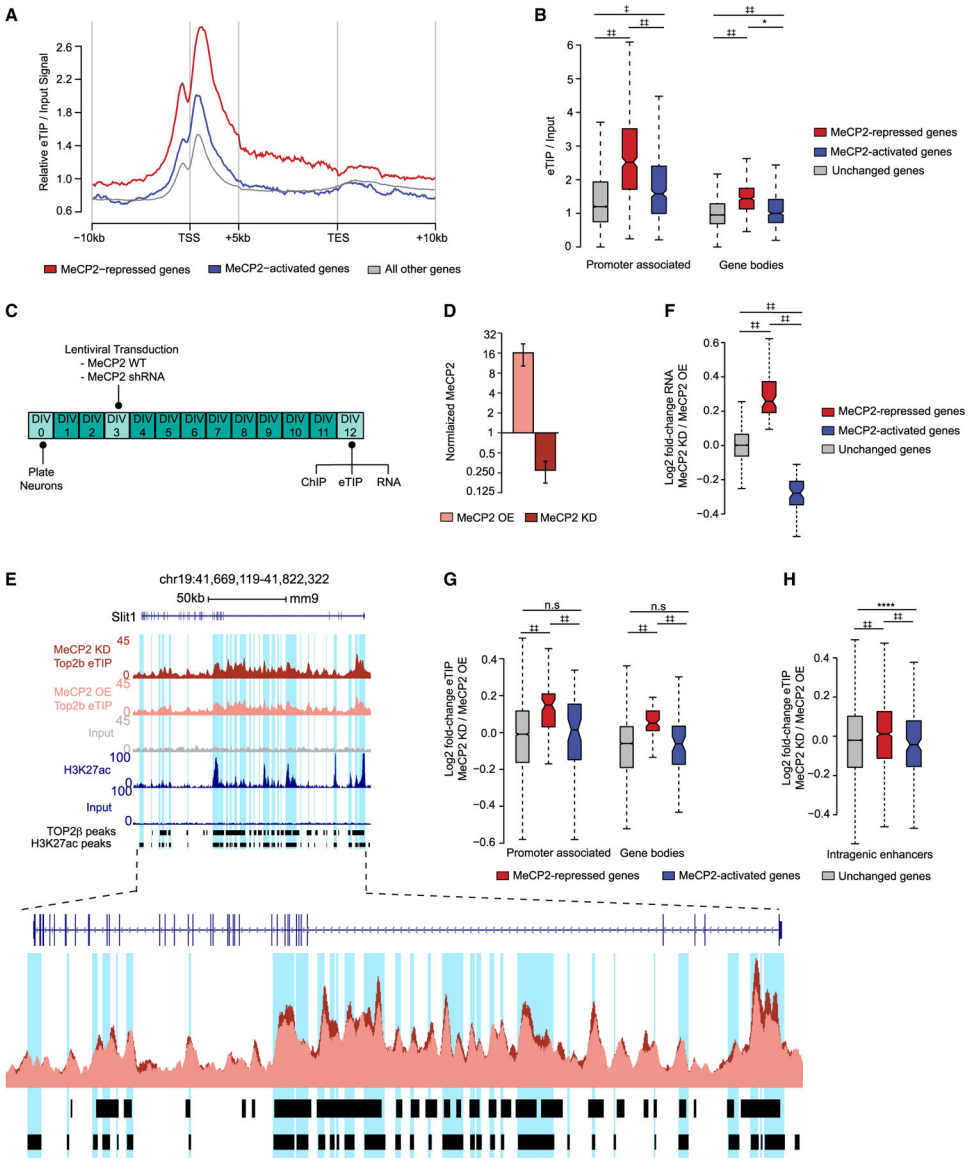

Figure 4. Altering MeCP2 levels in neurons affects TOP2β activity at MeCP2-regulated genes

(A) Aggregate plot of eTIP-seq in DIV12 cortical neuron cultures at MeCP2-repressed, MeCP2-activated, and all other genes as identified in studies of multiple MeCP2-mutant brain regions.[2] Data are from DIV12 primary neuron cultures. Wild-type eTIP-seq in (A) and (B), n = 4 biological replicates.

(B) Boxplot of eTIP signal at promoter-associated regions and gene bodies of MeCP2-repressed, MeCP2-activated, and all other genes. *$p < 0.05$; ‡$p < 10^{-9}$; ‡‡$p < 10^{-15}$; Wilcoxon rank-sum test.

(C) Experimental design to manipulate MeCP2 in cultured neurons and measure effects on TOP2β and mRNA expression.

(D) RT-qPCR of MeCP2 RNA expression in MeCP2-KD or -OE DIV12 neuron cultures, n = 3 biological replicates per group. MeCP2 expression mean ± SEM is normalized to *Actb* and control neurons lacking KD or OE.

(E) Genome browser snapshot of eTIP-seq signal at an example MeCP2-repressed gene, *Slit1*, in MeCP2-KD and -OE DIV12 neurons. Putative enhancers and promoter H3K27ac peaks are highlighted in blue. eTIP-seq track superimposition illustrates higher signal at this gene in MeCP2-KD compared with -OE. Data are from DIV12 primary neuron cultures. MeCP2-KD and -OE eTIP-seq in (E), (G), and (H), n = 4 biological replicates.

(F) Fold changes in exonic RNA between MeCP2-KD and -OE DIV12 cortical neurons. Gene sets were identified as MeCP2 repressed or MeCP2 activated across *in vivo* studies of MeCP2 mutants[2] and detected as significantly altered in these neuronal cultures upon MeCP2-KD or -OE (false discovery rate [FDR] < 0.1). ‡‡$p < 10^{-15}$; Wilcoxon rank-sum test. Data are from DIV12 primary neuron cultures. MeCP2-KD and -OE RNA-seq, n = 8 biological replicates.

(G) Fold changes calculated by edgeR analysis of eTIP-seq at promoter-associated regions and gene bodies in MeCP2-KD compared with -OE neurons for gene sets defined in (F). n.s., not significant; ‡‡$p< 10^{-15}$; Wilcoxon rank-sum test.

(H) Fold changes calculated by edgeR analysis of eTIP-seq in MeCP2-KD and -OE DIV12 neurons for enhancers located within gene sets defined in (F). ****$p < 0.0001$; ‡‡$p < 10^{-15}$; Wilcoxon rank-sum test.

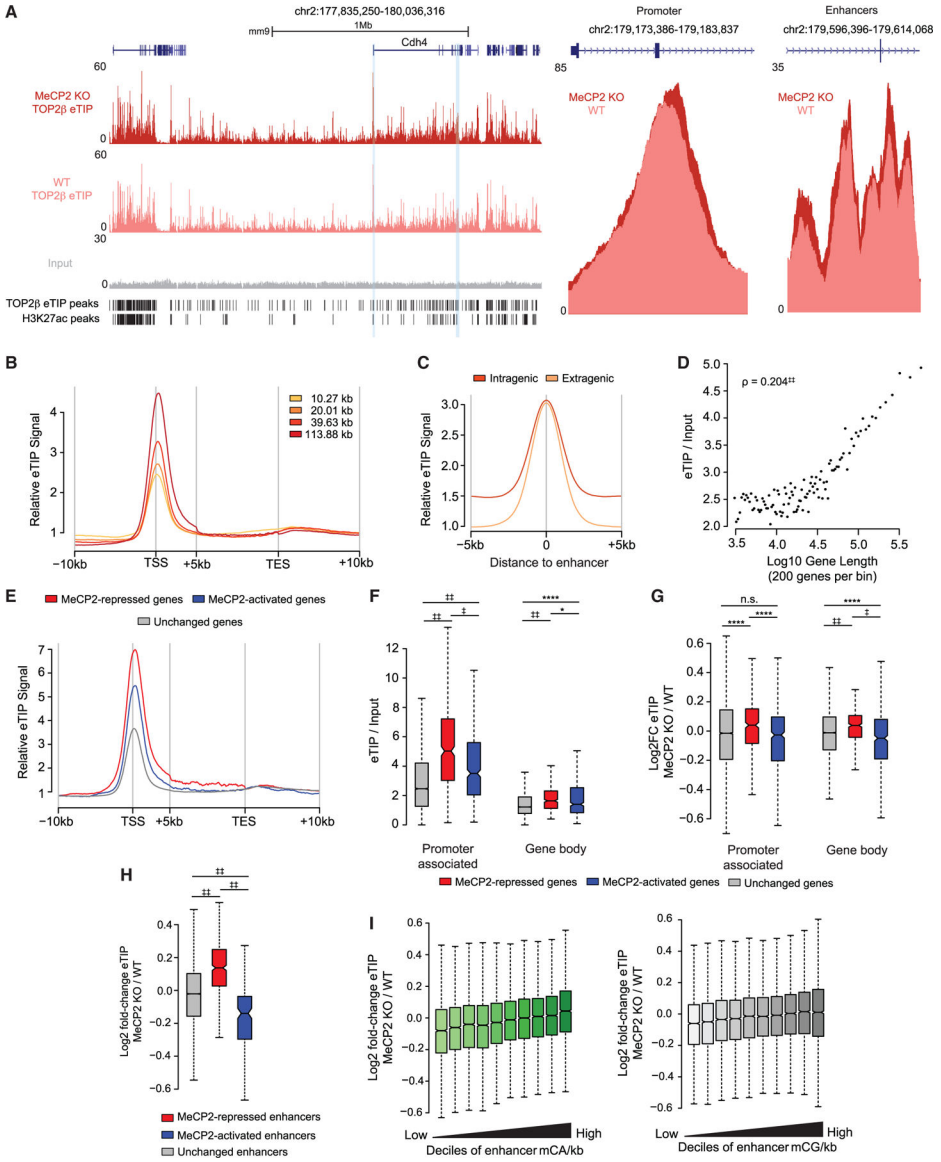

Figure 5. Knockout of MeCP2 leads to altered TOP2β in the adult cerebral cortex

(A) Left, genome browser view of eTIP-seq signal in cortical slices from adult wild-type and MeCP2-knockout (MeCP2-KO) mice at an example MeCP2-repressed gene, *Cdh4*. Putative enhancer and promoter H3K27ac peaks highlighted in blue are at higher resolution to the right. Right, superimposition of eTIP-seq tracks for *Cdh4* promoter and gene-associated enhancers showing higher signal in MeCP2 KO compared with the wild type. Data are from cerebral cortex of 8-week-old mice. eTIP-seq in (A) and (G) through (I), n = 3 biological replicates.

(B) Aggregate plot of eTIP signal from adult wild-type cortex at genes divided into gene length quantiles (see STAR Methods). The median gene length for each group is indicated. TSS, transcription start site; TES, transcription end site. Mean values are plotted for 100 bp bins. Data are from cerebral cortex of 8-week-old mice. eTIP-seq in (B) through (F), n = 2 biological replicates.

(C) Aggregate plot of eTIP signal at putative intragenic and extragenic enhancers genome wide in adult wild-type cortex. Putative enhancers are defined as H3K27ac peaks that do not overlap a gene TSS.[40] The plot is centered at the midpoint for each enhancer; mean values are plotted for 100 bp bins.

(D) Running average of eTIP signal at promoter-associated region for 200 gene bins ranked by gene length. Spearman rho is shown for gene length and eTIP signal. ‡‡$p < 10^{-15}$.

(E) Aggregate plot of eTIP signal in adult cortex at MeCP2-repressed, MeCP2-activated, and all other genes as identified in studies of multiple MeCP2-mutant brain regions.[2] Mean values are plotted for 100 bp bins.

(F) Boxplot of eTIP signal at promoter-associated regions and gene bodies of MeCP2-repressed, MeCP2-activated, and all other genes as described for (E). *$p < 0.05$; ****$p < 0.0001$; ‡$p < 10^{-9}$; ‡‡$p < 10^{-15}$; Wilcoxon rank-sum test.

(G) Fold changes calculated by edgeR analysis of eTIP-seq in promoter-associated regions and gene bodies in MeCP2 KO compared with control cortex for MeCP2-repressed and MeCP2-actived genes as described for (E). n.s., not significant; ****$p < 0.0001$; ‡$p < 10^{-9}$; ‡‡$p< 10^{-15}$; Wilcoxon rank-sum test.

(H) Fold changes calculated by edgeR analysis of eTIP-seq in MeCP2 KO compared with control cortex for MeCP2-repressed and MeCP2-actived genes for enhancers previously defined as regulated by MeCP2.[40] Fold changes were calculated by edgeR analysis of eTIP read counts at enhancer regions. ‡‡$p< 10^{-15}$; Wilcoxon rank-sum test.

(I) Fold changes calculated by edgeR analysis of eTIP-seq in MeCP2 KO compared with control cortex for all enhancers genome wide binned by their levels of DNA methylation, mCA and mCG. Spearman correlation significance: mCA, $p < 10^{-9}$; mCG, $p < 10^{-15}$. DNA-methylation data are from 8-week-old cerebral cortex.[70]

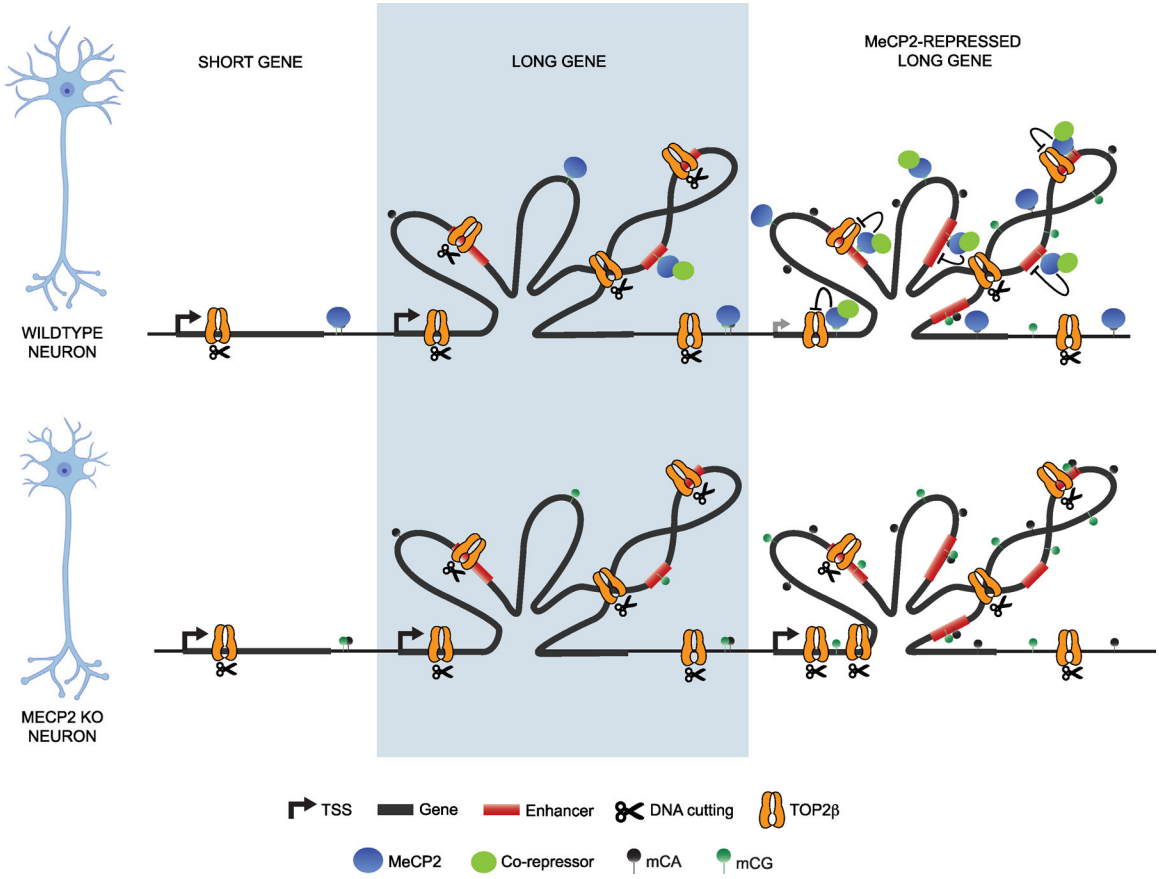

Figure 6. A model of MeCP2-mediated TOP2β activity in neurons

In neurons, TOP2β is preferentially recruited to promoter-associated regions, gene bodies, and enhancers of long genes, where it resolves topological constraints and facilitates gene expression. At long, MeCP2-repressed genes, DNA methylation and MeCP2 binding are enriched. MeCP2 interacts with TOP2β, acting as a molecular brake on topoisomerase activity to fine-tune the expression of these genes. When MeCP2 is absent, the TOP2β molecular brake is removed, causing TOP2β overactivity and overexpression of long, MeCP2-repressed genes.

KEY RESOURCES TABLE

REAGENT or RESOURCE	SOURCE	IDENTIFIER
Antibodies		
Rabbit polyclonal anti-MeCP2	Millipore Sigma	Cat# 07-013; RRID: AB_2144004
Mouse monoclonal anti-MeCP2	Millipore Sigma	Cat# M7443; RRID: AB_477235
Mouse monoclonal anti-Topo I (H-5)	Santa Cruz	Cat# sc-271285; RRID: AB_10611597
Rabbit polyclonal anti-Topo II-beta (H-286) [secondary]	Santa Cruz	Cat# sc-13059; RRID: AB_2205866
Rabbit polyclonal anti-Topo II-beta [primary]	Bethyl Laboratories	Cat# A300-950A; RRID: AB_805860
Rabbit polyclonal anti-Myc	Abcam	Cat# ab9106; RRID: AB_307014
Goat polyclonal anti-Myc	Abcam	Cat# ab9132; RRID: AB_307033
Mouse monoclonal anti-FLAG	Millipore Sigma	Cat# F3165; RRID: AB_259529
Rabbit monoclonal anti-alpha-Tubulin (EP1332Y)	Abcam	Cat# ab52866; RRID: AB_869989
Rabbit polyclonal anti-Histone H3 (acetyl K27)	Abcam	Cat# ab4729; RRID: AB_2118291
Anti-mouse IgG, HRP-linked	Cell Signaling Technologies	Cat# 7076; RRID: AB_330924
Anti-Rabbit IgG, HRP-linked	Cell Signaling Technologies	Cat# 7074; RRID: AB_2099233
Donkey-*anti*-Goat IgG, HRP	Thermo Fisher	Cat# A16005; RRID: AB_2534679
IRDye 800CW Donkey anti-Mouse	LI-COR	Cat# 926-32212; RRID: AB_621847
IRDye 800CW Donkey anti-Rabbit	LI-COR	Cat# 926-32213; RRID: AB_621848
IRDye 800CW Donkey anti-Goat	LI-COR	Cat# 926-32214; RRID: AB_621846
Bacterial and virus strains		
One Shot TOP10 Chemically Competent E. Coli	Thermo Fisher	Cat# C404010
One Shot Stbl3 Chemically Competent E. Coli	Thermo Fisher	Cat# C737303
Chemicals, peptides, and recombinant proteins		
Etoposide (VP-16)	Santa Cruz	Cat# sc-3512
Benzonase	Millipore Sigma	Cat# 71206
Dynabeads Protein A	Thermo Fisher	Cat# 10001D
Dynabeads Protein G	Thermo Fisher	Cat# 10003D
AMPure XP beads	Beckman Coulter	Cat# A63880
Critical commercial assays		
NotI (High Fidelity)	NEB	Cat# R3189
XhoI	NEB	Cat# R0146
Gibson Assembly	NEB	Cat# E5510
Q5 Hot Start High-Fidelity 2x Master Mix	NEB	Cat# M0494
RNeasy Mini Kit	Qiagen	Cat# 74104
Accel-NGS 2S Plus DNA Library Kit (24 rxns)	Swift Biosciences	Cat# 21024
2S Indexing Kit (12 indices, Set A)	Swift Biosciences	Cat# 26148
2S Indexing Kit (12 indices, Set B)	Swift Biosciences	Cat# 26248

REAGENT or RESOURCE	SOURCE	IDENTIFIER
Qubit dsDNA HS Assay Kit	Thermo Fisher	Cat# Q32854
NEBNext Ultra Directional RNA Library Prep Kit for Illumina	NEB	Cat# E7420S
NEBNext Mulitplex Oligos for Illumina (Index Primers Set 1)	NEB	Cat# E7335S
NEBNext rRNA Depletion Kit (Human/Mouse/Rat)	NEB	Cat# E6310L
Ovation Ultralow Library System V2	NuGEN	Cat# 0344-32
SignalFire ECL Reagent	Cell Signaling Technology	Cat# 6883
Deposited data		
Raw and analyzed data	This paper	GEO: GSE246463
Raw mass spectrometry data	This paper	PRIDE: PXD046904
Mus musculus mm9 genome assembly	UCSC	http://hgdownload.soe.ucsc.edu/goldenPath/mm9/
Ensembl gene models	UCSC	https://genome.ucsc.edu/cgi-bin/hgTables
Bisulfite-seq	Stroud et al., 2017[70]	GEO: GSE104298
MeCP2 ChIP-seq	Chen et al., 2015[32]	GEO: GSE66871
ChIP-sequencing data (H3K27ac)	Clemens et al., 2020[40]	GEO: GSE123373
MeCP2 mutant data	Gabel et al., 2015[2]	GEO: GSE60077
Experimental models: Cell lines		
HEK293T	ATCC	RRID:CVCL_0063
Experimental models: Organisms/strains		
Primary cortical neurons	Derived from E14.5 cortex dissected from pure C57BL6 mice (IMSR Cat# JAX:000664, RRID: IMSR_JAX:000664) obtained from the Jackson Laboratory.	JAX:000664, RRID: IMSR_JAX:000664
Mouse: C57BL/6J	The Jackson Laboratory	JAX:000664, RRID:IMSR_JAX:000664
Mouse: MeCP2 KO: B6.129P2(C)-MeCP2tm1.Bird/J	The Jackson Laboratory	JAX: 003890; RRID: IMSR_JAX:003890
Oligonucleotides		
qPCR primers (Table S5)	IDT	N/A
Recombinant DNA		
pBACh-TOP2B-Myc (full-length; WT)	This paper	N/A
pBACh-TOP2B-Myc (1-449 aa)	This paper	N/A
pBACh-TOP2B-Myc (450-1198 aa)	This paper	N/A
pBACh-TOP2B-Myc (1199-1612 aa)	This paper	N/A
p3xFLAG-CMV10-MeCP2 (full-length; WT)	Lyst et al., 2013[36]	N/A
p3xFLAG-CMV10-MeCP2 (1-484 aa)	Lyst et al., 2013[36]	N/A
p3xFLAG-CMV10-MeCP2 (1-167 aa)	Lyst et al., 2013[36]	N/A

REAGENT or RESOURCE	SOURCE	IDENTIFIER
p3xFLAG-CMV10-MeCP2 (143-484 aa)	Lyst et al., 2013[36]	N/A
p3xFLAG-CMV10-MeCP2 (308-484 aa)	Lyst et al., 2013[36]	N/A
U6-shRNA-Ubiquitin-MeCP2-IRES-GFP-FUGW	Zhou et al., 2006[78]	N/A
U6-MeCP2-shRNA-IRES-GFP-FUGW	Zhou et al., 2006[78]	N/A
U6-non-targeting-shRNA-IRES-GFP-FUGW	Zhou et al., 2006[78]	N/A
Ser312fs11x-FLAG-Dnmt3a-IRES-FUGW	Christian et al., 2020[79]	N/A
Tyr324Phe-Cre-IRES-GFP-FUGW	This paper	N/A
Software and algorithms		
DESeq2 (v1.14.1)	Love et al., 2014[80]	http://www.bioconductor.org/packages/release/bioc/html/DESeq2.html
edgeR (v3.16.5)	Robinson et al., 2009[81]	https://bioconductor.org/packages/release/bioc/html/edgeR.html
SAMtools (v1.3)	Li and Durbin, 2009[82]	https://sourceforge.net/projects/samtools/files/
BEDtools2 (v2.25.0)	Quinlan and Hall, 2010[83]	https://github.com/arq5x/bedtools2
Bowtie2 (v2.2.5)	Langmead and Salzberg, 2012[84]	http://bowtie-bio.sourceforge.net/bowtie2/index.shtml
STAR	Dobin et al., 2013[85]	https://github.com/alexdobin/STAR
fastQC		https://www.bioinformatics.babraham.ac.uk/projects/fastqc/
MACS2 (v2.1.0)	Zhang et al., 2008[86]	https://github.com/taoliu/MACS
Trim galore		https://www.bioinformatics.babraham.ac.uk/projects/trim_galore/